

UC Berkeley

UC Berkeley Previously Published Works

Title

Search for gravitational waves from Scorpius X-1 in the second Advanced LIGO observing run with an improved hidden Markov model

Permalink

<https://escholarship.org/uc/item/7pb4f3gm>

Journal

Physical Review D, 100(12)

ISSN

2470-0010

Authors

Abbott, BP
Abbott, R
Abbott, TD
[et al.](#)

Publication Date

2019-12-15

DOI

10.1103/physrevd.100.122002

Peer reviewed

Search for gravitational waves from Scorpius X-1 in the second Advanced LIGO observing run with an improved hidden Markov model

B. P. Abbott,¹ R. Abbott,¹ T. D. Abbott,² S. Abraham,³ F. Acernese,^{4,5} K. Ackley,⁶ C. Adams,⁷ R. X. Adhikari,¹ V. B. Adya,^{8,9} C. Affeldt,^{8,9} M. Agathos,¹⁰ K. Agatsuma,¹¹ N. Aggarwal,¹² O. D. Aguiar,¹³ L. Aiello,^{14,15} A. Ain,³ P. Ajith,¹⁶ G. Allen,¹⁷ A. Allocca,^{18,19} M. A. Aloy,²⁰ P. A. Altin,²¹ A. Amato,²² A. Ananyeva,¹ S. B. Anderson,¹ W. G. Anderson,²³ S. V. Angelova,²⁴ S. Antier,²⁵ S. Appert,¹ K. Arai,¹ M. C. Araya,¹ J. S. Areeda,²⁶ M. Arène,²⁷ N. Arnaud,^{25,28} S. Ascenzi,^{29,30} G. Ashton,⁶ S. M. Aston,⁷ P. Astone,³¹ F. Aubin,³² P. Aufmuth,⁹ K. AultONeal,³³ C. Austin,² V. Avendano,³⁴ A. Avila-Alvarez,²⁶ S. Babak,^{35,27} P. Bacon,²⁷ F. Badaracco,^{14,15} M. K. M. Bader,³⁶ S. Bae,³⁷ P. T. Baker,³⁸ F. Baldaccini,^{39,40} G. Ballardín,²⁸ S. W. Ballmer,⁴¹ S. Banagiri,⁴² J. C. Barayoga,¹ S. E. Barclay,⁴³ B. C. Barish,¹ D. Barker,⁴⁴ K. Barkett,⁴⁵ S. Barnum,¹² F. Barone,^{4,5} B. Barr,⁴³ L. Barsotti,¹² M. Barsuglia,²⁷ D. Barta,⁴⁶ J. Bartlett,⁴⁴ I. Bartos,⁴⁷ R. Bassiri,⁴⁸ A. Basti,^{18,19} M. Bawaj,^{49,40} J. C. Bayley,⁴³ M. Bazzan,^{50,51} B. Bécsy,⁵² M. Bejger,^{27,53} I. Belahcene,²⁵ A. S. Bell,⁴³ D. Beniwal,⁵⁴ B. K. Berger,⁴⁸ G. Bergmann,^{8,9} S. Bernuzzi,^{55,56} J. J. Bero,⁵⁷ C. P. L. Berry,⁵⁸ D. Bersanetti,⁵⁹ A. Bertolini,³⁶ J. Betzwieser,⁷ R. Bhandare,⁶⁰ J. Bidler,²⁶ I. A. Bilenko,⁶¹ S. A. Bilgili,³⁸ G. Billingsley,¹ J. Birch,⁷ R. Birney,²⁴ O. Birnholtz,⁵⁷ S. Biscans,^{1,12} S. Biscoveanu,⁶ A. Bisht,⁹ M. Bitossi,^{28,19} M. A. Bizouard,²⁵ J. K. Blackburn,¹ C. D. Blair,⁷ D. G. Blair,⁶² R. M. Blair,⁴⁴ S. Bloemen,⁶³ N. Bode,^{8,9} M. Boer,⁶⁴ Y. Boetzel,⁶⁵ G. Bogaert,⁶⁴ F. Bondu,⁶⁶ E. Bonilla,⁴⁸ R. Bonnard,³² P. Booker,^{8,9} B. A. Boom,³⁶ C. D. Booth,⁶⁷ R. Bork,¹ V. Boschi,²⁸ S. Bose,^{68,3} K. Bossie,⁷ V. Bossilkov,⁶² J. Bosveld,⁶² Y. Bouffanaïs,²⁷ A. Bozzi,²⁸ C. Bradaschia,¹⁹ P. R. Brady,²³ A. Bramley,⁷ M. Branchesi,^{14,15} J. E. Brau,⁶⁹ T. Briant,⁷⁰ J. H. Briggs,⁴³ F. Brighenti,^{71,72} A. Brillet,⁶⁴ M. Brinkmann,^{8,9} V. Brisson,^{25,*} P. Brockill,²³ A. F. Brooks,¹ D. D. Brown,⁵⁴ S. Brunett,¹ A. Buikema,¹² T. Bulik,⁷³ H. J. Bulten,^{74,36} A. Buonanno,^{35,75} D. Buskulic,³² C. Buy,²⁷ R. L. Byer,⁴⁸ M. Cabero,^{8,9} L. Cadonati,⁷⁶ G. Cagnoli,^{22,77} C. Cahillane,¹ J. Calderón Bustillo,⁶ T. A. Callister,¹ E. Calloni,^{78,5} J. B. Camp,⁷⁹ W. A. Campbell,⁶ M. Canepa,^{80,59} K. C. Cannon,⁸¹ H. Cao,⁵⁴ J. Cao,⁸² E. Capocasa,²⁷ F. Carbognani,²⁸ S. Caride,⁸³ M. F. Carney,⁵⁸ G. Carullo,¹⁸ J. Casanueva Diaz,¹⁹ C. Casentini,^{29,30} S. Caudill,³⁶ M. Cavaglià,⁸⁴ F. Cavalier,²⁵ R. Cavalieri,²⁸ G. Cella,¹⁹ P. Cerdá-Durán,²⁰ G. Cerretani,^{18,19} E. Cesarini,^{85,30} O. Chaibi,⁶⁴ K. Chakravarti,³ S. J. Chamberlin,⁸⁶ M. Chan,⁴³ S. Chao,⁸⁷ P. Charlton,⁸⁸ E. A. Chase,⁵⁸ E. Chassande-Mottin,²⁷ D. Chatterjee,²³ M. Chaturvedi,⁶⁰ B. D. Cheeseboro,³⁸ H. Y. Chen,⁸⁹ X. Chen,⁶² Y. Chen,⁴⁵ H.-P. Cheng,⁴⁷ C. K. Cheong,⁹⁰ H. Y. Chia,⁴⁷ A. Chincarini,⁵⁹ A. Chiummo,²⁸ G. Cho,⁹¹ H. S. Cho,⁹² M. Cho,⁷⁵ N. Christensen,^{64,93} Q. Chu,⁶² S. Chua,⁷⁰ K. W. Chung,⁹⁰ S. Chung,⁶² G. Ciani,^{50,51} A. A. Ciobanu,⁵⁴ R. Ciolfi,^{94,95} F. Cipriano,⁶⁴ A. Cirone,^{80,59} F. Clara,⁴⁴ J. A. Clark,⁷⁶ P. Clearwater,⁹⁶ F. Cleva,⁶⁴ C. Cocchieri,⁸⁴ E. Coccia,^{14,15} P.-F. Cohadon,⁷⁰ D. Cohen,²⁵ R. Colgan,⁹⁷ M. Colleoni,⁹⁸ C. G. Collette,⁹⁹ C. Collins,¹¹ L. R. Cominsky,¹⁰⁰ M. Constancio Jr.,¹³ L. Conti,⁵¹ S. J. Cooper,¹¹ P. Corban,⁷ T. R. Corbitt,² I. Cordero-Carrión,¹⁰¹ K. R. Corley,⁹⁷ N. Cornish,⁵² A. Corsi,⁸³ S. Cortese,²⁸ C. A. Costa,¹³ R. Cotesta,³⁵ M. W. Coughlin,¹ S. B. Coughlin,^{67,58} J.-P. Coulon,⁶⁴ S. T. Countryman,⁹⁷ P. Couvares,¹ P. B. Covas,⁹⁸ E. E. Cowan,⁷⁶ D. M. Coward,⁶² M. J. Cowart,⁷ D. C. Coyne,¹ R. Coyne,¹⁰² J. D. E. Creighton,²³ T. D. Creighton,¹⁰³ J. Cripe,² M. Croquette,⁷⁰ S. G. Crowder,¹⁰⁴ T. J. Cullen,² A. Cumming,⁴³ L. Cunningham,⁴³ E. Cuoco,²⁸ T. Dal Canton,⁷⁹ G. Dálya,¹⁰⁵ S. L. Danilishin,^{8,9} S. D'Antonio,³⁰ K. Danzmann,^{9,8} A. Dasgupta,¹⁰⁶ C. F. Da Silva Costa,⁴⁷ L. E. H. Datrier,⁴³ V. Dattilo,²⁸ I. Dave,⁶⁰ M. Davier,²⁵ D. Davis,⁴¹ E. J. Daw,¹⁰⁷ D. DeBra,⁴⁸ M. Deenadayalan,³ J. Degallaix,²² M. De Laurentis,^{78,5} S. Deléglise,⁷⁰ W. Del Pozzo,^{18,19} L. M. DeMarchi,⁵⁸ N. Demos,¹² T. Dent,^{8,9,108} R. De Pietri,^{109,56} J. Derby,²⁶ R. De Rosa,^{78,5} C. De Rossi,^{22,28} R. DeSalvo,¹¹⁰ O. de Varona,^{8,9} S. Dhurandhar,³ M. C. Díaz,¹⁰³ T. Dietrich,³⁶ L. Di Fiore,⁵ M. Di Giovanni,^{111,95} T. Di Girolamo,^{78,5} A. Di Lieto,^{18,19} B. Ding,⁹⁹ S. Di Pace,^{112,31} I. Di Palma,^{112,31} F. Di Renzo,^{18,19} A. Dmitriev,¹¹ Z. Doctor,⁸⁹ F. Donovan,¹² K. L. Dooley,^{67,84} S. Doravari,^{8,9} I. Dorrington,⁶⁷ T. P. Downes,²³ M. Drago,^{14,15} J. C. Driggers,⁴⁴ Z. Du,⁸² J.-G. Ducoin,²⁵ P. Dupej,⁴³ S. E. Dwyer,⁴⁴ P. J. Easter,⁶ T. B. Edo,¹⁰⁷ M. C. Edwards,⁹³ A. Effler,⁷ P. Ehrens,¹ J. Eichholz,¹ S. S. Eikenberry,⁴⁷ M. Eisenmann,³² R. A. Eisenstein,¹² R. C. Essick,⁸⁹ H. Estelles,⁹⁸ D. Estevez,³² Z. B. Etienne,³⁸ T. Etzel,¹ M. Evans,¹² T. M. Evans,⁷ V. Fafone,^{29,30,14} H. Fair,⁴¹ S. Fairhurst,⁶⁷ X. Fan,⁸² S. Farinon,⁵⁹ B. Farr,⁶⁹ W. M. Farr,¹¹ E. J. Fauchon-Jones,⁶⁷ M. Favata,³⁴ M. Fays,¹⁰⁷ M. Fazio,¹¹³ C. Fee,¹¹⁴ J. Feicht,¹ M. M. Fejer,⁴⁸ F. Feng,²⁷ A. Fernandez-Galiana,¹² I. Ferrante,^{18,19} E. C. Ferreira,¹³ T. A. Ferreira,¹³ F. Ferrini,²⁸ F. Fidecaro,^{18,19} I. Fiori,²⁸ D. Fiorucci,²⁷ M. Fishbach,⁸⁹ R. P. Fisher,^{41,115} J. M. Fishner,¹² M. Fitz-Axen,⁴² R. Flaminio,^{32,116} M. Fletcher,⁴³ E. Flynn,²⁶ H. Fong,¹¹⁷ J. A. Font,^{20,118} P. W. F. Forsyth,²¹ J.-D. Fournier,⁶⁴ S. Frasca,^{112,31} F. Frasconi,¹⁹ Z. Frei,¹⁰⁵ A. Freise,¹¹ R. Frey,⁶⁹ V. Frey,²⁵ P. Fritschel,¹² V. V. Frolov,⁷ P. Fulda,⁴⁷ M. Fyffe,⁷ H. A. Gabbard,⁴³

- B. U. Gadre,³ S. M. Gaebel,¹¹ J. R. Gair,¹¹⁹ L. Gammaitoni,³⁹ M. R. Ganija,⁵⁴ S. G. Gaonkar,³ A. Garcia,²⁶
 C. García-Quirós,⁹⁸ F. Garufi,^{78,5} B. Gateley,⁴⁴ S. Gaudio,³³ G. Gaur,¹²⁰ V. Gayathri,¹²¹ G. Gemme,⁵⁹
 E. Genin,²⁸ A. Gennai,¹⁹ D. George,¹⁷ J. George,⁶⁰ L. Gergely,¹²² V. Germain,³² S. Ghonge,⁷⁶ Abhirup Ghosh,¹⁶
 Archisman Ghosh,³⁶ S. Ghosh,²³ B. Giacomazzo,^{111,95} J. A. Giaime,^{2,7} K. D. Giardino,⁷ A. Giazotto,^{19,†}
 K. Gill,³³ G. Giordano,^{4,5} L. Glover,¹¹⁰ P. Godwin,⁸⁶ E. Goetz,⁴⁴ R. Goetz,⁴⁷ B. Goncharov,⁶ G. González,²
 J. M. Gonzalez Castro,^{18,19} A. Gopakumar,¹²³ M. L. Gorodetsky,⁶¹ S. E. Gossan,¹ M. Gosselin,²⁸ R. Gouaty,³²
 A. Grado,^{124,5} C. Graef,⁴³ M. Granata,²² A. Grant,⁴³ S. Gras,¹² P. Grassia,¹ C. Gray,⁴⁴ R. Gray,⁴³
 G. Greco,^{71,72} A. C. Green,^{11,47} R. Green,⁶⁷ E. M. Gretarsson,³³ P. Groot,⁶³ H. Grote,⁶⁷ S. Grunewald,³⁵
 P. Gruning,²⁵ G. M. Guidi,^{71,72} H. K. Gulati,¹⁰⁶ Y. Guo,³⁶ A. Gupta,⁸⁶ M. K. Gupta,¹⁰⁶ E. K. Gustafson,¹
 R. Gustafson,¹²⁵ L. Haegel,⁹⁸ O. Halim,^{15,14} B. R. Hall,⁶⁸ E. D. Hall,¹² E. Z. Hamilton,⁶⁷ G. Hammond,⁴³
 M. Haney,⁶⁵ M. M. Hanke,^{8,9} J. Hanks,⁴⁴ C. Hanna,⁸⁶ M. D. Hannam,⁶⁷ O. A. Hannuksela,⁹⁰ J. Hanson,⁷
 T. Hardwick,² K. Haris,¹⁶ J. Harms,^{14,15} G. M. Harry,¹²⁶ I. W. Harry,³⁵ C.-J. Haster,¹¹⁷ K. Haughian,⁴³
 F. J. Hayes,⁴³ J. Healy,⁵⁷ A. Heidmann,⁷⁰ M. C. Heintze,⁷ H. Heitmann,⁶⁴ P. Hello,²⁵ G. Hemming,²⁸
 M. Hendry,⁴³ I. S. Heng,⁴³ J. Hennig,^{8,9} A. W. Heptonstall,¹ Francisco Hernandez Vivanco,⁶ M. Heurs,^{8,9}
 S. Hild,⁴³ T. Hinderer,^{127,36,128} D. Hoak,²⁸ S. Hochheim,^{8,9} D. Hofman,²² A. M. Holgado,¹⁷ N. A. Holland,²¹
 K. Holt,⁷ D. E. Holz,⁸⁹ P. Hopkins,⁶⁷ C. Horst,²³ J. Hough,⁴³ E. J. Howell,⁶² C. G. Hoy,⁶⁷ A. Hreibi,⁶⁴
 E. A. Huerta,¹⁷ D. Huet,²⁵ B. Hughey,³³ M. Hulko,¹ S. Husa,⁹⁸ S. H. Huttner,⁴³ T. Huynh-Dinh,⁷ B. Idzkowski,⁷³
 A. Iess,^{29,30} C. Ingram,⁵⁴ R. Inta,⁸³ G. Intini,^{112,31} B. Irwin,¹¹⁴ H. N. Isa,⁴³ J.-M. Isac,⁷⁰ M. Isi,¹ B. R. Iyer,¹⁶
 K. Izumi,⁴⁴ T. Jacqmin,⁷⁰ S. J. Jadhav,¹²⁹ K. Jani,⁷⁶ N. N. Janthalur,¹²⁹ P. Jananowski,¹³⁰ A. C. Jenkins,¹³¹
 J. Jiang,⁴⁷ D. S. Johnson,¹⁷ A. W. Jones,¹¹ D. I. Jones,¹³² R. Jones,⁴³ R. J. G. Jonker,³⁶ L. Ju,⁶² J. Junker,^{8,9}
 C. V. Kalaghatgi,⁶⁷ V. Kalogera,⁵⁸ B. Kamai,¹ S. Kandhasamy,⁸⁴ G. Kang,³⁷ J. B. Kanner,¹ S. J. Kapadia,²³
 S. Karki,⁶⁹ K. S. Karvinen,^{8,9} R. Kashyap,¹⁶ M. Kasprzak,¹ S. Katsanevas,²⁸ E. Katsavounidis,¹² W. Katzman,⁷
 S. Kaufer,⁹ K. Kawabe,⁴⁴ N. V. Keerthana,³ F. Kéfélian,⁶⁴ D. Keitel,⁴³ R. Kennedy,¹⁰⁷ J. S. Key,¹³³ F. Y. Khalili,⁶¹
 H. Khan,²⁶ I. Khan,^{14,30} S. Khan,^{8,9} Z. Khan,¹⁰⁶ E. A. Khazanov,¹³⁴ M. Khursheed,⁶⁰ N. Kijbunchoo,²¹
 Chunglee Kim,¹³⁵ J. C. Kim,¹³⁶ K. Kim,⁹⁰ W. Kim,⁵⁴ W. S. Kim,¹³⁷ Y.-M. Kim,¹³⁸ C. Kimball,⁵⁸ E. J. King,⁵⁴
 P. J. King,⁴⁴ M. Kinley-Hanlon,¹²⁶ R. Kirchhoff,^{8,9} J. S. Kissel,⁴⁴ L. Kleybolte,¹³⁹ J. H. Klika,²³ S. Klimentko,⁴⁷
 T. D. Knowles,³⁸ P. Koch,^{8,9} S. M. Koehlenbeck,^{8,9} G. Koekoek,^{36,140} S. Koley,³⁶ V. Kondrashov,¹ A. Kontos,¹²
 N. Koper,^{8,9} M. Korobko,¹³⁹ W. Z. Korth,¹ I. Kowalska,⁷³ D. B. Kozak,¹ V. Kringel,^{8,9} N. Krishnendu,¹⁴¹
 A. Królak,^{142,143} G. Kuehn,^{8,9} A. Kumar,¹²⁹ P. Kumar,¹⁴⁴ R. Kumar,¹⁰⁶ S. Kumar,¹⁶ L. Kuo,⁸⁷ A. Kutynia,¹⁴²
 S. Kwang,²³ B. D. Lackey,³⁵ K. H. Lai,⁹⁰ T. L. Lam,⁹⁰ M. Landry,⁴⁴ B. B. Lane,¹² R. N. Lang,¹⁴⁵ J. Lange,⁵⁷
 B. Lantz,⁴⁸ R. K. Lanza,¹² A. Lartaux-Vollard,²⁵ P. D. Lasky,⁶ M. Laxen,⁷ A. Lazzarini,¹ C. Lazzaro,⁵¹
 P. Leaci,^{112,31} S. Leavey,^{8,9} Y. K. Lecoeuche,⁴⁴ C. H. Lee,⁹² H. K. Lee,¹⁴⁶ H. M. Lee,¹⁴⁷ H. W. Lee,¹³⁶
 J. Lee,⁹¹ K. Lee,⁴³ J. Lehmann,^{8,9} A. Lenon,³⁸ N. Leroy,²⁵ N. Letendre,³² Y. Levin,^{6,97} J. Li,⁸² K. J. L. Li,⁹⁰
 T. G. F. Li,⁹⁰ X. Li,⁴⁵ F. Lin,⁶ F. Linde,³⁶ S. D. Linker,¹¹⁰ T. B. Littenberg,¹⁴⁸ J. Liu,⁶² X. Liu,²³ R. K. L. Lo,^{90,1}
 N. A. Lockerbie,²⁴ L. T. London,⁶⁷ A. Longo,^{149,150} M. Lorenzini,^{14,15} V. Lorette,¹⁵¹ M. Lormand,⁷
 G. Losurdo,¹⁹ J. D. Lough,^{8,9} C. O. Lousto,⁵⁷ G. Lovelace,²⁶ M. E. Lower,¹⁵² H. Lück,^{9,8} D. Lumaca,^{29,30}
 A. P. Lundgren,¹⁵³ R. Lynch,¹² Y. Ma,⁴⁵ R. Macas,⁶⁷ S. Macfoy,²⁴ M. MacInnis,¹² D. M. Macleod,⁶⁷
 A. Macquet,⁶⁴ F. Magaña-Sandoval,⁴¹ L. Magaña Zertuche,⁸⁴ R. M. Magee,⁸⁶ E. Majorana,³¹ I. Maksimovic,¹⁵¹
 A. Malik,⁶⁰ N. Man,⁶⁴ V. Mandic,⁴² V. Mangano,⁴³ G. L. Mansell,^{44,12} M. Manske,^{23,21} M. Mantovani,²⁸
 F. Marchesoni,^{49,40} F. Marion,³² S. Márka,⁹⁷ Z. Márka,⁹⁷ C. Markakis,^{10,17} A. S. Markosyan,⁴⁸ A. Markowitz,¹
 E. Maros,¹ A. Marquina,¹⁰¹ S. Marsat,³⁵ F. Martelli,^{71,72} I. W. Martin,⁴³ R. M. Martin,³⁴ D. V. Martynov,¹¹
 K. Mason,¹² E. Massera,¹⁰⁷ A. Masserot,³² T. J. Massinger,¹ M. Masso-Reid,⁴³ S. Mastrogiovanni,^{112,31}
 A. Matas,^{42,35} F. Matichard,^{1,12} L. Matone,⁹⁷ N. Mavalvala,¹² N. Mazumder,⁶⁸ J. J. McCann,⁶² R. McCarthy,⁴⁴
 D. E. McClelland,²¹ S. McCormick,⁷ L. McCuller,¹² S. C. McGuire,¹⁵⁴ J. McIver,¹ D. J. McManus,²¹ T. McRae,²¹
 S. T. McWilliams,³⁸ D. Meacher,⁸⁶ G. D. Meadors,⁶ M. Mehmet,^{8,9} A. K. Mehta,¹⁶ J. Meidam,³⁶ A. Melatos,⁹⁶
 G. Mendell,⁴⁴ R. A. Mercer,²³ L. Mereni,²² E. L. Merilh,⁴⁴ M. Merzougui,⁶⁴ S. Meshkov,¹ C. Messenger,⁴³
 C. Messick,⁸⁶ R. Metzdrorf,⁷⁰ P. M. Meyers,⁹⁶ H. Miao,¹¹ C. Michel,²² H. Middleton,⁹⁶ E. E. Mikhailov,¹⁵⁵
 L. Milano,^{78,5} A. L. Miller,⁴⁷ A. Miller,^{112,31} M. Millhouse,⁵² J. C. Mills,⁶⁷ M. C. Milovich-Goff,¹¹⁰
 O. Minazzoli,^{64,156} Y. Minenkov,³⁰ A. Mishkin,⁴⁷ C. Mishra,¹⁵⁷ T. Mistry,¹⁰⁷ S. Mitra,³ V. P. Mitrofanov,⁶¹
 G. Mitselmakher,⁴⁷ R. Mittleman,¹² G. Mo,⁹³ D. Moffa,¹¹⁴ K. Mogushi,⁸⁴ S. R. P. Mohapatra,¹² M. Montani,^{71,72}
 C. J. Moore,¹⁰ D. Moraru,⁴⁴ G. Moreno,⁴⁴ S. Morisaki,⁸¹ B. Mours,³² C. M. Mow-Lowry,¹¹ Arunava Mukherjee,^{8,9}
 D. Mukherjee,²³ S. Mukherjee,¹⁰³ N. Mukund,³ A. Mullavey,⁷ J. Munch,⁵⁴ E. A. Muñiz,⁴¹ M. Muratore,³³
 P. G. Murray,⁴³ A. Nagar,^{85,158,159} I. Nardecchia,^{29,30} L. Naticchioni,^{112,31} R. K. Nayak,¹⁶⁰ J. Neilson,¹¹⁰

- G. Nelemans,^{63,36} T. J. N. Nelson,⁷ M. Nery,^{8,9} A. Neunzert,¹²⁵ K. Y. Ng,¹² S. Ng,⁵⁴ P. Nguyen,⁶⁹ D. Nichols,^{127,36} S. Nissanke,^{127,36} F. Nocera,²⁸ C. North,⁶⁷ L. K. Nuttall,¹⁵³ M. Obergaulinger,²⁰ J. Oberling,⁴⁴ B. D. O'Brien,⁴⁷ G. D. O'Dea,¹¹⁰ G. H. Ogin,¹⁶¹ J. J. Oh,¹³⁷ S. H. Oh,¹³⁷ F. Ohme,^{8,9} H. Ohta,⁸¹ M. A. Okada,¹³ M. Oliver,⁹⁸ P. Oppermann,^{8,9} Richard J. Oram,⁷ B. O'Reilly,⁷ R. G. Ormiston,⁴² L. F. Ortega,⁴⁷ R. O'Shaughnessy,⁵⁷ S. Ossokine,³⁵ D. J. Ottaway,⁵⁴ H. Overmier,⁷ B. J. Owen,⁸³ A. E. Pace,⁸⁶ G. Pagano,^{18,19} M. A. Page,⁶² A. Pai,¹²¹ S. A. Pai,⁶⁰ J. R. Palamos,⁶⁹ O. Palashov,¹³⁴ C. Palomba,³¹ A. Pal-Singh,¹³⁹ Huang-Wei Pan,⁸⁷ B. Pang,⁴⁵ P. T. H. Pang,⁹⁰ C. Pankow,⁵⁸ F. Pannarale,^{112,31} B. C. Pant,⁶⁰ F. Paoletti,¹⁹ A. Paoli,²⁸ A. Parida,³ W. Parker,^{7,154} D. Pascucci,⁴³ A. Pasqualetti,²⁸ R. Passaquieti,^{18,19} D. Passuello,¹⁹ M. Patil,¹⁴³ B. Patricelli,^{18,19} B. L. Pearlstone,⁴³ C. Pedersen,⁶⁷ M. Pedraza,¹ R. Pedurand,^{22,162} A. Pele,⁷ S. Penn,¹⁶³ C. J. Perez,⁴⁴ A. Perreca,^{111,95} H. P. Pfeiffer,^{35,117} M. Phelps,^{8,9} K. S. Phukon,³ O. J. Piccinni,^{112,31} M. Pichot,⁶⁴ F. Piergiovanni,^{71,72} G. Pillant,²⁸ L. Pinard,²² M. Pirello,⁴⁴ M. Pitkin,⁴³ R. Poggiani,^{18,19} D. Y. T. Pong,⁹⁰ S. Ponrathnam,³ P. Popolizio,²⁸ E. K. Porter,²⁷ J. Powell,¹⁵² A. K. Prajapati,¹⁰⁶ J. Prasad,³ K. Prasai,⁴⁸ R. Prasanna,¹²⁹ G. Pratten,⁹⁸ T. Prestegard,²³ S. Privitera,³⁵ G. A. Prodi,^{111,95} L. G. Prokhorov,⁶¹ O. Puncken,^{8,9} M. Punturo,⁴⁰ P. Puppo,³¹ M. Pürerer,³⁵ H. Qi,²³ V. Quetschke,¹⁰³ P. J. Quinonez,³³ E. A. Quintero,¹ R. Quitzow-James,⁶⁹ F. J. Raab,⁴⁴ H. Radkins,⁴⁴ N. Radulescu,⁶⁴ P. Raffai,¹⁰⁵ S. Raja,⁶⁰ C. Rajan,⁶⁰ B. Rajbhandari,⁸³ M. Rakhmanov,¹⁰³ K. E. Ramirez,¹⁰³ A. Ramos-Buades,⁹⁸ Javed Rana,³ K. Rao,⁵⁸ P. Rapagnani,^{112,31} V. Raymond,⁶⁷ M. Razzano,^{18,19} J. Read,²⁶ T. Regimbau,³² L. Rei,⁵⁹ S. Reid,²⁴ D. H. Reitze,^{1,47} W. Ren,¹⁷ F. Ricci,^{112,31} C. J. Richardson,³³ J. W. Richardson,¹ P. M. Ricker,¹⁷ K. Riles,¹²⁵ M. Rizzo,⁵⁸ N. A. Robertson,^{1,43} R. Robie,⁴³ F. Robinet,²⁵ A. Rocchi,³⁰ L. Rolland,³² J. G. Rollins,¹ V. J. Roma,⁶⁹ M. Romanelli,⁶⁶ R. Romano,^{4,5} C. L. Romel,⁴⁴ J. H. Romie,⁷ K. Rose,¹¹⁴ D. Rosińska,^{164,53} S. G. Rosofsky,¹⁷ M. P. Ross,¹⁶⁵ S. Rowan,⁴³ A. Rüdiger,^{8,9,†} P. Ruggi,²⁸ G. Rutins,¹⁶⁶ K. Ryan,⁴⁴ S. Sachdev,¹ T. Sadecki,⁴⁴ M. Sakellariadou,¹³¹ L. Salconi,²⁸ M. Saleem,¹⁴¹ A. Samajdar,³⁶ L. Sammut,⁶ E. J. Sanchez,¹ L. E. Sanchez,¹ N. Sanchis-Gual,²⁰ V. Sandberg,⁴⁴ J. R. Sanders,⁴¹ K. A. Santiago,³⁴ N. Sarin,⁶ B. Sassolas,²² P. R. Saulson,⁴¹ O. Sauter,¹²⁵ R. L. Savage,⁴⁴ P. Schale,⁶⁹ M. Scheel,⁴⁵ J. Scheuer,⁵⁸ P. Schmidt,⁶³ R. Schnabel,¹³⁹ R. M. S. Schofield,⁶⁹ A. Schönbeck,¹³⁹ E. Schreiber,^{8,9} B. W. Schulte,^{8,9} B. F. Schutz,⁶⁷ S. G. Schwalbe,³³ J. Scott,⁴³ S. M. Scott,²¹ E. Seidel,¹⁷ D. Sellers,⁷ A. S. Sengupta,¹⁶⁷ N. Sennett,³⁵ D. Sentenac,²⁸ V. Sequino,^{29,30,14} A. Sergeev,¹³⁴ Y. Setyawati,^{8,9} D. A. Shaddock,²¹ T. Shaffer,⁴⁴ M. S. Shahriar,⁵⁸ M. B. Shaner,¹¹⁰ L. Shao,³⁵ P. Sharma,⁶⁰ P. Shawhan,⁷⁵ H. Shen,¹⁷ R. Shink,¹⁶⁸ D. H. Shoemaker,¹² D. M. Shoemaker,⁷⁶ S. ShyamSundar,⁶⁰ K. Siellez,⁷⁶ M. Sieniawska,⁵³ D. Sigg,⁴⁴ A. D. Silva,¹³ L. P. Singer,⁷⁹ N. Singh,⁷³ A. Singhal,^{14,31} A. M. Sintès,⁹⁸ S. Sitmukhambetov,¹⁰³ V. Skliris,⁶⁷ B. J. J. Slagmolen,²¹ T. J. Slaven-Blair,⁶² J. R. Smith,²⁶ R. J. E. Smith,⁶ S. Somala,¹⁶⁹ E. J. Son,¹³⁷ B. Sorazu,⁴³ F. Sorrentino,⁵⁹ T. Souradeep,³ E. Sowell,⁸³ A. P. Spencer,⁴³ A. K. Srivastava,¹⁰⁶ V. Srivastava,⁴¹ K. Staats,⁵⁸ C. Stachie,⁶⁴ M. Standke,^{8,9} D. A. Steer,²⁷ M. Steinke,^{8,9} J. Steinlechner,^{139,43} S. Steinlechner,¹³⁹ D. Steinmeyer,^{8,9} S. P. Stevenson,¹⁵² D. Stocks,⁴⁸ R. Stone,¹⁰³ D. J. Stops,¹¹ K. A. Strain,⁴³ G. Stratta,^{71,72} S. E. Strigin,⁶¹ A. Strunk,⁴⁴ R. Sturani,¹⁷⁰ A. L. Stuver,¹⁷¹ V. Sudhir,¹² T. Z. Summerscales,¹⁷² L. Sun,¹ S. Sunil,¹⁰⁶ J. Suresh,³ P. J. Sutton,⁶⁷ B. L. Swinkels,³⁶ M. J. Szczepańczyk,³³ M. Tacca,³⁶ S. C. Tait,⁴³ C. Talbot,⁶ D. Talukder,⁶⁹ D. B. Tanner,⁴⁷ M. Tápai,¹²² A. Taracchini,³⁵ J. D. Tasson,⁹³ R. Taylor,¹ F. Thies,^{8,9} M. Thomas,⁷ P. Thomas,⁴⁴ S. R. Thondapu,⁶⁰ K. A. Thorne,⁷ E. Thrane,⁶ Shubhanshu Tiwari,^{111,95} Srishti Tiwari,¹²³ V. Tiwari,⁶⁷ K. Toland,⁴³ M. Tonelli,^{18,19} Z. Tornasi,⁴³ A. Torres-Forné,¹⁷³ C. I. Torrie,¹ D. Töyrä,¹¹ F. Travasso,^{28,40} G. Traylor,⁷ M. C. Tringali,⁷³ A. Trovato,²⁷ L. Trozzo,^{174,19} R. Trudeau,¹ K. W. Tsang,³⁶ M. Tse,¹² R. Tso,⁴⁵ L. Tsukada,⁸¹ D. Tsuna,⁸¹ D. Tuyenbayev,¹⁰³ K. Ueno,⁸¹ D. Ugolini,¹⁷⁵ C. S. Unnikrishnan,¹²³ A. L. Urban,² S. A. Usman,⁶⁷ H. Vahlbruch,⁹ G. Vajente,¹ G. Valdes,² N. van Bakel,³⁶ M. van Beuzekom,³⁶ J. F. J. van den Brand,^{74,36} C. Van Den Broeck,^{36,176} D. C. Vander-Hyde,⁴¹ J. V. van Heijningen,⁶² L. van der Schaaf,³⁶ A. A. van Veggel,⁴³ M. Vardaro,^{50,51} V. Varma,⁴⁵ S. Vass,¹ M. Vasúth,⁴⁶ A. Vecchio,¹¹ G. Vedovato,⁵¹ J. Veitch,⁴³ P. J. Veitch,⁵⁴ K. Venkateswara,¹⁶⁵ G. Venugopalan,¹ D. Verkindt,³² F. Vetrano,^{71,72} A. Viceré,^{71,72} A. D. Viets,²³ D. J. Vine,¹⁶⁶ J.-Y. Vinet,⁶⁴ S. Vitale,¹² T. Vo,⁴¹ H. Vocca,^{39,40} C. Vorvick,⁴⁴ S. P. Vyatchanin,⁶¹ A. R. Wade,¹ L. E. Wade,¹¹⁴ M. Wade,¹¹⁴ R. Walet,³⁶ M. Walker,²⁶ L. Wallace,¹ S. Walsh,²³ G. Wang,^{14,19} H. Wang,¹¹ J. Z. Wang,¹²⁵ W. H. Wang,¹⁰³ Y. F. Wang,⁹⁰ R. L. Ward,²¹ Z. A. Warden,³³ J. Warner,⁴⁴ M. Was,³² J. Watchi,⁹⁹ B. Weaver,⁴⁴ L.-W. Wei,^{8,9} M. Weinert,^{8,9} A. J. Weinstein,¹ R. Weiss,¹² F. Wellmann,^{8,9} L. Wen,⁶² E. K. Wessel,¹⁷ P. Weßels,^{8,9} J. W. Westhouse,³³ K. Wette,²¹ J. T. Whelan,⁵⁷ B. F. Whiting,⁴⁷ C. Whittle,¹² D. M. Wilken,^{8,9} D. Williams,⁴³ A. R. Williamson,^{127,36} J. L. Willis,¹ B. Willke,^{8,9} M. H. Wimmer,^{8,9} W. Winkler,^{8,9} C. C. Wipf,¹ H. Wittel,^{8,9} G. Woan,⁴³ J. Woehler,^{8,9} J. K. Wofford,⁵⁷ J. Worden,⁴⁴ J. L. Wright,⁴³ D. S. Wu,^{8,9} D. M. Wysocki,⁵⁷ L. Xiao,¹ H. Yamamoto,¹ C. C. Yancey,⁷⁵ L. Yang,¹¹³ M. J. Yap,²¹ M. Yazback,⁴⁷ D. W. Yeeles,⁶⁷ Hang Yu,¹² Haocun Yu,¹²

S. H. R. Yuen,⁹⁰ M. Yvert,³² A. K. Zdrożny,^{103,142} M. Zanolin,³³ T. Zelenova,²⁸ J.-P. Zendri,⁵¹ M. Zevin,⁵⁸
 J. Zhang,⁶² L. Zhang,¹ T. Zhang,⁴³ C. Zhao,⁶² M. Zhou,⁵⁸ Z. Zhou,⁵⁸ X. J. Zhu,⁶ M. E. Zucker,^{1,12} and J. Zweizig¹
 (The LIGO Scientific Collaboration and the Virgo Collaboration)

L. M. Dunn,⁹⁶ S. Suvorova,⁹⁶ R. J. Evans,⁹⁶ and W. Moran⁹⁶

¹LIGO, California Institute of Technology, Pasadena, CA 91125, USA

²Louisiana State University, Baton Rouge, LA 70803, USA

³Inter-University Centre for Astronomy and Astrophysics, Pune 411007, India

⁴Università di Salerno, Fisciano, I-84084 Salerno, Italy

⁵INFN, Sezione di Napoli, Complesso Universitario di Monte S. Angelo, I-80126 Napoli, Italy

⁶OzGrav, School of Physics & Astronomy, Monash University, Clayton 3800, Victoria, Australia

⁷LIGO Livingston Observatory, Livingston, LA 70754, USA

⁸Max Planck Institute for Gravitational Physics (Albert Einstein Institute), D-30167 Hannover, Germany

⁹Leibniz Universität Hannover, D-30167 Hannover, Germany

¹⁰University of Cambridge, Cambridge CB2 1TN, United Kingdom

¹¹University of Birmingham, Birmingham B15 2TT, United Kingdom

¹²LIGO, Massachusetts Institute of Technology, Cambridge, MA 02139, USA

¹³Instituto Nacional de Pesquisas Espaciais, 12227-010 São José dos Campos, São Paulo, Brazil

¹⁴Gran Sasso Science Institute (GSSI), I-67100 L'Aquila, Italy

¹⁵INFN, Laboratori Nazionali del Gran Sasso, I-67100 Assergi, Italy

¹⁶International Centre for Theoretical Sciences, Tata Institute of Fundamental Research, Bengaluru 560089, India

¹⁷NCSA, University of Illinois at Urbana-Champaign, Urbana, IL 61801, USA

¹⁸Università di Pisa, I-56127 Pisa, Italy

¹⁹INFN, Sezione di Pisa, I-56127 Pisa, Italy

²⁰Departamento de Astronomía y Astrofísica, Universitat de València, E-46100 Burjassot, València, Spain

²¹OzGrav, Australian National University, Canberra, Australian Capital Territory 0200, Australia

²²Laboratoire des Matériaux Avancés (LMA), CNRS/IN2P3, F-69622 Villeurbanne, France

²³University of Wisconsin-Milwaukee, Milwaukee, WI 53201, USA

²⁴SUPA, University of Strathclyde, Glasgow G1 1XQ, United Kingdom

²⁵LAL, Univ. Paris-Sud, CNRS/IN2P3, Université Paris-Saclay, F-91898 Orsay, France

²⁶California State University Fullerton, Fullerton, CA 92831, USA

²⁷APC, AstroParticule et Cosmologie, Université Paris Diderot,

CNRS/IN2P3, CEA/Irfu, Observatoire de Paris,

Sorbonne Paris Cité, F-75205 Paris Cedex 13, France

²⁸European Gravitational Observatory (EGO), I-56021 Cascina, Pisa, Italy

²⁹Università di Roma Tor Vergata, I-00133 Roma, Italy

³⁰INFN, Sezione di Roma Tor Vergata, I-00133 Roma, Italy

³¹INFN, Sezione di Roma, I-00185 Roma, Italy

³²Laboratoire d'Annecy de Physique des Particules (LAPP), Univ. Grenoble Alpes,

Université Savoie Mont Blanc, CNRS/IN2P3, F-74941 Annecy, France

³³Embry-Riddle Aeronautical University, Prescott, AZ 86301, USA

³⁴Montclair State University, Montclair, NJ 07043, USA

³⁵Max Planck Institute for Gravitational Physics (Albert Einstein Institute), D-14476 Potsdam-Golm, Germany

³⁶Nikhef, Science Park 105, 1098 XG Amsterdam, The Netherlands

³⁷Korea Institute of Science and Technology Information, Daejeon 34141, South Korea

³⁸West Virginia University, Morgantown, WV 26506, USA

³⁹Università di Perugia, I-06123 Perugia, Italy

⁴⁰INFN, Sezione di Perugia, I-06123 Perugia, Italy

⁴¹Syracuse University, Syracuse, NY 13244, USA

⁴²University of Minnesota, Minneapolis, MN 55455, USA

⁴³SUPA, University of Glasgow, Glasgow G12 8QQ, United Kingdom

⁴⁴LIGO Hanford Observatory, Richland, WA 99352, USA

⁴⁵Caltech CaRT, Pasadena, CA 91125, USA

⁴⁶Wigner RCP, RMKI, H-1121 Budapest, Konkoly Thege Miklós út 29-33, Hungary

⁴⁷University of Florida, Gainesville, FL 32611, USA

⁴⁸Stanford University, Stanford, CA 94305, USA

⁴⁹Università di Camerino, Dipartimento di Fisica, I-62032 Camerino, Italy

⁵⁰Università di Padova, Dipartimento di Fisica e Astronomia, I-35131 Padova, Italy

⁵¹INFN, Sezione di Padova, I-35131 Padova, Italy

⁵²Montana State University, Bozeman, MT 59717, USA

⁵³Nicolaus Copernicus Astronomical Center, Polish Academy of Sciences, 00-716, Warsaw, Poland

⁵⁴OzGrav, University of Adelaide, Adelaide, South Australia 5005, Australia

- ⁵⁵ *Theoretisch-Physikalisches Institut, Friedrich-Schiller-Universität Jena, D-07743 Jena, Germany*
- ⁵⁶ *INFN, Sezione di Milano Bicocca, Gruppo Collegato di Parma, I-43124 Parma, Italy*
- ⁵⁷ *Rochester Institute of Technology, Rochester, NY 14623, USA*
- ⁵⁸ *Center for Interdisciplinary Exploration & Research in Astrophysics (CIERA), Northwestern University, Evanston, IL 60208, USA*
- ⁵⁹ *INFN, Sezione di Genova, I-16146 Genova, Italy*
- ⁶⁰ *RRCAT, Indore, Madhya Pradesh 452013, India*
- ⁶¹ *Faculty of Physics, Lomonosov Moscow State University, Moscow 119991, Russia*
- ⁶² *OzGrav, University of Western Australia, Crawley, Western Australia 6009, Australia*
- ⁶³ *Department of Astrophysics/IMAPP, Radboud University Nijmegen, P.O. Box 9010, 6500 GL Nijmegen, The Netherlands*
- ⁶⁴ *Artemis, Université Côte d'Azur, Observatoire Côte d'Azur, CNRS, CS 34229, F-06304 Nice Cedex 4, France*
- ⁶⁵ *Physik-Institut, University of Zurich, Winterthurerstrasse 190, 8057 Zurich, Switzerland*
- ⁶⁶ *Univ Rennes, CNRS, Institut FOTON - UMR6082, F-3500 Rennes, France*
- ⁶⁷ *Cardiff University, Cardiff CF24 3AA, United Kingdom*
- ⁶⁸ *Washington State University, Pullman, WA 99164, USA*
- ⁶⁹ *University of Oregon, Eugene, OR 97403, USA*
- ⁷⁰ *Laboratoire Kastler Brossel, Sorbonne Université, CNRS, ENS-Université PSL, Collège de France, F-75005 Paris, France*
- ⁷¹ *Università degli Studi di Urbino 'Carlo Bo,' I-61029 Urbino, Italy*
- ⁷² *INFN, Sezione di Firenze, I-50019 Sesto Fiorentino, Firenze, Italy*
- ⁷³ *Astronomical Observatory Warsaw University, 00-478 Warsaw, Poland*
- ⁷⁴ *VU University Amsterdam, 1081 HV Amsterdam, The Netherlands*
- ⁷⁵ *University of Maryland, College Park, MD 20742, USA*
- ⁷⁶ *School of Physics, Georgia Institute of Technology, Atlanta, GA 30332, USA*
- ⁷⁷ *Université Claude Bernard Lyon 1, F-69622 Villeurbanne, France*
- ⁷⁸ *Università di Napoli 'Federico II,' Complesso Universitario di Monte S. Angelo, I-80126 Napoli, Italy*
- ⁷⁹ *NASA Goddard Space Flight Center, Greenbelt, MD 20771, USA*
- ⁸⁰ *Dipartimento di Fisica, Università degli Studi di Genova, I-16146 Genova, Italy*
- ⁸¹ *RESCEU, University of Tokyo, Tokyo, 113-0033, Japan.*
- ⁸² *Tsinghua University, Beijing 100084, China*
- ⁸³ *Texas Tech University, Lubbock, TX 79409, USA*
- ⁸⁴ *The University of Mississippi, University, MS 38677, USA*
- ⁸⁵ *Museo Storico della Fisica e Centro Studi e Ricerche "Enrico Fermi", I-00184 Roma, Italyrico Fermi, I-00184 Roma, Italy*
- ⁸⁶ *The Pennsylvania State University, University Park, PA 16802, USA*
- ⁸⁷ *National Tsing Hua University, Hsinchu City, 30013 Taiwan, Republic of China*
- ⁸⁸ *Charles Sturt University, Wagga Wagga, New South Wales 2678, Australia*
- ⁸⁹ *University of Chicago, Chicago, IL 60637, USA*
- ⁹⁰ *The Chinese University of Hong Kong, Shatin, NT, Hong Kong*
- ⁹¹ *Seoul National University, Seoul 08826, South Korea*
- ⁹² *Pusan National University, Busan 46241, South Korea*
- ⁹³ *Carleton College, Northfield, MN 55057, USA*
- ⁹⁴ *INAF, Osservatorio Astronomico di Padova, I-35122 Padova, Italy*
- ⁹⁵ *INFN, Trento Institute for Fundamental Physics and Applications, I-38123 Povo, Trento, Italy*
- ⁹⁶ *OzGrav, University of Melbourne, Parkville, Victoria 3010, Australia*
- ⁹⁷ *Columbia University, New York, NY 10027, USA*
- ⁹⁸ *Universitat de les Illes Balears, IAC3—IEEC, E-07122 Palma de Mallorca, Spain*
- ⁹⁹ *Université Libre de Bruxelles, Brussels 1050, Belgium*
- ¹⁰⁰ *Sonoma State University, Rohnert Park, CA 94928, USA*
- ¹⁰¹ *Departamento de Matemáticas, Universitat de València, E-46100 Burjassot, València, Spain*
- ¹⁰² *University of Rhode Island, Kingston, RI 02881, USA*
- ¹⁰³ *The University of Texas Rio Grande Valley, Brownsville, TX 78520, USA*
- ¹⁰⁴ *Bellevue College, Bellevue, WA 98007, USA*
- ¹⁰⁵ *MTA-ELTE Astrophysics Research Group, Institute of Physics, Eötvös University, Budapest 1117, Hungary*
- ¹⁰⁶ *Institute for Plasma Research, Bhat, Gandhinagar 382428, India*
- ¹⁰⁷ *The University of Sheffield, Sheffield S10 2TN, United Kingdom*
- ¹⁰⁸ *IGFAE, Campus Sur, Universidad de Santiago de Compostela, 15782 Spain*
- ¹⁰⁹ *Dipartimento di Scienze Matematiche, Fisiche e Informatiche, Università di Parma, I-43124 Parma, Italy*
- ¹¹⁰ *California State University, Los Angeles, 5151 State University Dr, Los Angeles, CA 90032, USA*
- ¹¹¹ *Università di Trento, Dipartimento di Fisica, I-38123 Povo, Trento, Italy*
- ¹¹² *Università di Roma 'La Sapienza,' I-00185 Roma, Italy*
- ¹¹³ *Colorado State University, Fort Collins, CO 80523, USA*

- ¹¹⁴Kenyon College, Gambier, OH 43022, USA
- ¹¹⁵Christopher Newport University, Newport News, VA 23606, USA
- ¹¹⁶National Astronomical Observatory of Japan, 2-21-1 Osawa, Mitaka, Tokyo 181-8588, Japan
- ¹¹⁷Canadian Institute for Theoretical Astrophysics,
University of Toronto, Toronto, Ontario M5S 3H8, Canada
- ¹¹⁸Observatori Astronòmic, Universitat de València, E-46980 Paterna, València, Spain
- ¹¹⁹School of Mathematics, University of Edinburgh, Edinburgh EH9 3FD, United Kingdom
- ¹²⁰Institute Of Advanced Research, Gandhinagar 382426, India
- ¹²¹Indian Institute of Technology Bombay, Powai, Mumbai 400 076, India
- ¹²²University of Szeged, Dóm tér 9, Szeged 6720, Hungary
- ¹²³Tata Institute of Fundamental Research, Mumbai 400005, India
- ¹²⁴INAF, Osservatorio Astronomico di Capodimonte, I-80131, Napoli, Italy
- ¹²⁵University of Michigan, Ann Arbor, MI 48109, USA
- ¹²⁶American University, Washington, D.C. 20016, USA
- ¹²⁷GRAPPA, Anton Pannekoek Institute for Astronomy and Institute of High-Energy Physics,
University of Amsterdam, Science Park 904, 1098 XH Amsterdam, The Netherlands
- ¹²⁸Delta Institute for Theoretical Physics, Science Park 904, 1090 GL Amsterdam, The Netherlands
- ¹²⁹Directorate of Construction, Services & Estate Management, Mumbai 400094 India
- ¹³⁰University of Białystok, 15-424 Białystok, Poland
- ¹³¹King's College London, University of London, London WC2R 2LS, United Kingdom
- ¹³²University of Southampton, Southampton SO17 1BJ, United Kingdom
- ¹³³University of Washington Bothell, Bothell, WA 98011, USA
- ¹³⁴Institute of Applied Physics, Nizhny Novgorod, 603950, Russia
- ¹³⁵Ewha Womans University, Seoul 03760, South Korea
- ¹³⁶Inje University Gimhae, South Gyeongsang 50834, South Korea
- ¹³⁷National Institute for Mathematical Sciences, Daejeon 34047, South Korea
- ¹³⁸Ulsan National Institute of Science and Technology, Ulsan 44919, South Korea
- ¹³⁹Universität Hamburg, D-22761 Hamburg, Germany
- ¹⁴⁰Maastricht University, P.O. Box 616, 6200 MD Maastricht, The Netherlands
- ¹⁴¹Chennai Mathematical Institute, Chennai 603103, India
- ¹⁴²NCBJ, 05-400 Świerk-Otwock, Poland
- ¹⁴³Institute of Mathematics, Polish Academy of Sciences, 00656 Warsaw, Poland
- ¹⁴⁴Cornell University, Ithaca, NY 14850, USA
- ¹⁴⁵Hillsdale College, Hillsdale, MI 49242, USA
- ¹⁴⁶Hanyang University, Seoul 04763, South Korea
- ¹⁴⁷Korea Astronomy and Space Science Institute, Daejeon 34055, South Korea
- ¹⁴⁸NASA Marshall Space Flight Center, Huntsville, AL 35811, USA
- ¹⁴⁹Dipartimento di Matematica e Fisica, Università degli Studi Roma Tre, I-00146 Roma, Italy
- ¹⁵⁰INFN, Sezione di Roma Tre, I-00146 Roma, Italy
- ¹⁵¹ESPCI, CNRS, F-75005 Paris, France
- ¹⁵²OzGrav, Swinburne University of Technology, Hawthorn VIC 3122, Australia
- ¹⁵³University of Portsmouth, Portsmouth, PO1 3FX, United Kingdom
- ¹⁵⁴Southern University and A&M College, Baton Rouge, LA 70813, USA
- ¹⁵⁵College of William and Mary, Williamsburg, VA 23187, USA
- ¹⁵⁶Centre Scientifique de Monaco, 8 quai Antoine 1er, MC-98000, Monaco
- ¹⁵⁷Indian Institute of Technology Madras, Chennai 600036, India
- ¹⁵⁸INFN Sezione di Torino, Via P. Giuria 1, I-10125 Torino, Italy
- ¹⁵⁹Institut des Hautes Etudes Scientifiques, F-91440 Bures-sur-Yvette, France
- ¹⁶⁰IISER-Kolkata, Mohanpur, West Bengal 741252, India
- ¹⁶¹Whitman College, 345 Boyer Avenue, Walla Walla, WA 99362 USA
- ¹⁶²Université de Lyon, F-69361 Lyon, France
- ¹⁶³Hobart and William Smith Colleges, Geneva, NY 14456, USA
- ¹⁶⁴Janusz Gil Institute of Astronomy, University of Zielona Góra, 65-265 Zielona Góra, Poland
- ¹⁶⁵University of Washington, Seattle, WA 98195, USA
- ¹⁶⁶SUPA, University of the West of Scotland, Paisley PA1 2BE, United Kingdom
- ¹⁶⁷Indian Institute of Technology, Gandhinagar Ahmedabad Gujarat 382424, India
- ¹⁶⁸Université de Montréal/Polytechnique, Montreal, Quebec H3T 1J4, Canada
- ¹⁶⁹Indian Institute of Technology Hyderabad, Sangareddy, Khandi, Telangana 502285, India
- ¹⁷⁰International Institute of Physics, Universidade Federal do Rio Grande do Norte, Natal RN 59078-970, Brazil
- ¹⁷¹Villanova University, 800 Lancaster Ave, Villanova, PA 19085, USA
- ¹⁷²Andrews University, Berrien Springs, MI 49104, USA
- ¹⁷³Max Planck Institute for Gravitationalphysik (Albert Einstein Institute), D-14476 Potsdam-Golm, Germany
- ¹⁷⁴Università di Siena, I-53100 Siena, Italy
- ¹⁷⁵Trinity University, San Antonio, TX 78212, USA

¹⁷⁶ *Van Swinderen Institute for Particle Physics and Gravity,
University of Groningen, Nijenborgh 4, 9747 AG Groningen, The Netherlands*

We present results from a semicoherent search for continuous gravitational waves from the low-mass X-ray binary Scorpius X-1, using a hidden Markov model (HMM) to track spin wandering. This search improves on previous HMM-based searches of LIGO data by using an improved frequency domain matched filter, the \mathcal{J} -statistic, and by analysing data from Advanced LIGO's second observing run. In the frequency range searched, from 60 to 650 Hz, we find no evidence of gravitational radiation. At 194.6 Hz, the most sensitive search frequency, we report an upper limit on gravitational wave strain (at 95% confidence) of $h_0^{95\%} = 3.47 \times 10^{-25}$ when marginalising over source inclination angle. This is the most sensitive search for Scorpius X-1, to date, that is specifically designed to be robust in the presence of spin wandering.

I. INTRODUCTION

Rotating neutron stars with non-axisymmetric deformations are predicted to emit persistent, periodic gravitational radiation. They are a key target for continuous-wave searches performed with gravitational wave (GW) detectors such as the second-generation Advanced Laser Interferometer Gravitational-wave Observatory (Advanced LIGO) [1–5] and Virgo [4]. The time-varying quadrupole moment necessary for GW emission may result from thermal [6, 7], or magnetic [8–10] gradients, r -modes [11–13], or nonaxisymmetric circulation of the superfluid interior [14–17]. These mechanisms produce signals at certain multiples of the spin frequency f_* [1]. Of particular interest are accreting low-mass X-ray binaries (LMXB), such as Scorpius X-1 (Sco X-1), where a neutron star is spun up by accretion from its stellar companion. Electromagnetic observations of LMXBs to date imply $f_* \lesssim 620$ Hz [18], well short of the theoretical centrifugal break-up limit $f_* \lesssim 1.5$ kHz [19]. Regardless of the exact GW mechanism, the latter observation suggests an equilibrium between the spin-up accretion torque, and GW spin-down torque [20–22]. Torque balance also implies a relation between X-ray luminosity and the GW strain, making Sco X-1, the brightest LMXB X-ray source, the most promising known target.

Initial LIGO, a first-generation detector, started taking science data in 2002. It reached its design sensitivity in Science Run 5 (S5), starting 2005 [23], and exceeded it in Science Run 6 (S6) [24]. Following detector upgrades, the second-generation Advanced LIGO interferometer [2] began taking science data during Observing Run 1 (O1), which ran from September 2015 to January 2016. The strain noise in O1 is three to four times lower than S6 between 100 Hz and 300 Hz [25]. During this period, LIGO observed three binary black hole mergers, GW150914 [26], GW151012 and GW151226 [27]. Observing Run 2 (O2) began on November 2016, and ran until 26 August 2017. From 1 August 2017, the two LIGO detectors were joined by Virgo, resulting in a three-detector network.

As well as further binary black hole mergers [28], LIGO and Virgo made the first gravitational wave observation of a binary neutron-star merger during O2 [29].

No search has yet reported a detection of a continuous wave source. To date, four searches for Sco X-1 have been conducted on Initial LIGO data, and three on Advanced LIGO data. The first search coherently analysed the most-sensitive six hour segment from Science Run 2 (S2) using the \mathcal{F} -statistic [30], a maximum likelihood detection statistic [31]. The second was a directed, semicoherent analysis using the \mathcal{C} -statistic [32]. The third, also a directed analysis, used the TwoSpect algorithm on doubly Fourier transformed S5 data [33–35]. The fourth applied the radiometer algorithm [36] to conduct a directed search on S4 [37], S5 [38], and later O1 [39] data. Three LMXB searches have been performed with Advanced LIGO data, comprising the radiometer search [39], an analysis based on a hidden Markov model (HMM) [40], and a cross-correlation analysis [41–43]. The upper limits established by these searches are summarized in Table I.

Astrophysical modeling and X-ray observations suggest that the spin frequency of an LMXB wanders stochastically in response to fluctuations in the hydro-magnetic accretion torque [44–47]. As no electromagnetic measurements of f_* are available to guide a gravitational wave search for Sco X-1, such searches must either account for spin wandering or limit their observing times and/or coherence times in accordance with the anticipated timescale and amplitude of the spin wandering [48]. For example, the sideband search described in Ref. [32] is restricted to data segments no longer than ten days. The hidden Markov model (HMM) tracker, first applied to the search for Sco X-1 in Ref. [40], is an effective technique for detecting the most probable underlying spin frequency, $f_*(t)$ and thus accounting for spin wandering.

The signal from a binary source is Doppler shifted, as the neutron star revolves around the barycentre of the binary, dispersing power into orbital sidebands near the source frame emission frequency. The separation of these sidebands and the source-frame frequency depends on the binary orbital parameters and f , but is typically within 0.05 per cent of the gravitational wave frequency for a source such as Sco X-1. Four maximum-likelihood matched filters have been developed to detect these sidebands: the \mathcal{C} -statistic, which weights sidebands equally

* Deceased, February 2018.

† Deceased, November 2017.

‡ Deceased, July 2018.

[32], the binary modulated \mathcal{F} -statistic [49], the Bessel-weighted \mathcal{F} -statistic [50], and the \mathcal{J} -statistic, which extends the Bessel-weighted \mathcal{F} -statistic to account for the phase of the binary orbit [51]. Any of these matched filters can be combined with the HMM to conduct a search for signals from a binary source that accounts for spin wandering.

In this paper, we combine the \mathcal{J} -statistic described in Ref. [51] with the HMM described in that paper and Refs. [50] and [40], and perform a directed search of Advanced LIGO O2 data for evidence of a gravitational wave signal from Sco X-1. In the search band 60–650 Hz, we find no evidence of a gravitational wave signal. The paper is organized as follows. In Section II, we briefly review the HMM and the \mathcal{J} -statistic. In Section III, we discuss the search strategy and parameter space. In Section IV, we report on the results from the search and veto candidates corresponding to instrumental artifacts. In Section V, we discuss the search sensitivity and consequent upper limits on the gravitational wave strain.

II. SEARCH ALGORITHM

In this section, we outline the two key components of the search algorithm: the HMM, used to recover the most probable spin history $f_0(t)$, and the \mathcal{J} -statistic, the matched filter that accounts for the Doppler shifts introduced by the orbital motions of the Earth and the LMXB. The HMM formalism is the same as used in Refs. [40, 50, 51], so we review it only briefly. The \mathcal{J} -statistic is described fully in Ref. [51]; again, we review it briefly.

A. HMM formalism

A Markov model describes a stochastic process in terms of a state variable $q(t)$, which transitions between allowable states $\{q_1, \dots, q_{N_Q}\}$ at discrete times $\{t_0, \dots, t_{N_T}\}$. The transition matrix $A_{q_j q_i}$ represents the probability of jumping from state q_i at the time $t = t_n$ to q_j at $t = t_{n+1}$ depending only on $q(t_n)$. A HMM extends the Markov model to situations where direct observation of $q(t)$ is impossible [$q(t)$ is called the hidden state]. Instead one measures an observable state $o(t)$, selected from $\{o_1, \dots, o_{N_o}\}$, which is related to the hidden state by the emission matrix $L_{o_j q_i}$, which gives the likelihood that the system is in state q_i given the observation o_j . In gravitational wave searches for LMXBs like Sco X-1, where the spin frequency cannot be measured electromagnetically, it is natural to map $q(t)$ to $f_0(t)$ and $o(t)$ to the raw interferometer data, some equivalent intermediate data product (e.g. short Fourier transforms), or a detection statistic (e.g., \mathcal{F} -statistic, \mathcal{J} -statistic).

In an LMXB search, we divide the total observation (duration T_{obs}) into N_T equal segments of length $T_{\text{drift}} = T_{\text{obs}}/N_T$. In practice, T_{drift} is chosen on astro-

physical grounds to give $N_T = \lceil T_{\text{obs}}/T_{\text{drift}} \rceil$ based on an estimates of plausible spin-wandering timescales [48]; in this paper we follow Ref. [40] in choosing $T_{\text{drift}} = 10$ d. The tracker is able to track the signal even if the spin frequency occasionally jumps by two bins as it can catch up to the signal path, although with an attendant loss of sensitivity as the recovered must include a step that contains only noise.

In each segment, the emission probability $L_{o_j q_i}$ is computed from some frequency domain estimator $G(f)$ such as the maximum likelihood \mathcal{F} - or \mathcal{J} -statistic (discussed in Section II B). The frequency resolution of the estimator is $\Delta f_{\text{drift}} = 1/(2T_{\text{drift}})$. The probability that an observation $O = \{o(t_1), \dots, o(t_{N_T})\}$ is associated with a particular hidden path $Q = \{q(t_0), \dots, q(t_{N_T})\}$ is then given by:

$$P(Q|O) \propto L_{o(t_{N_T})q(t_{N_T})} A_{q(t_{N_T})q(t_{N_T-1})} \cdots L_{o(t_1)q(t_1)} \times A_{q(t_1)q(t_0)} \Pi_{q(t_0)}, \quad (1)$$

where Π_{q_i} is the prior, i.e., the probability the system starts in state q_i at $t = t_0$. For this search, we take a flat prior. (Note that there is no initial observation $o(t_0)$ as the initial state of the system is captured by the prior.) The task, then, is to find the optimal hidden path Q^* , that is, the path Q^* that maximizes $P(Q|O)$ given O . We find Q^* efficiently with the recursive Viterbi algorithm [54], which is discussed in detail in Appendix A of Ref. [40].

In this paper, we follow the convention in Ref. [40] of defining the Viterbi detection score S for a path as the number of standard deviations by which that path's log likelihood exceeds the mean log likelihood of all paths. Mathematically we have

$$S = \frac{\ln \delta_{q^*}(t_{N_T}) - \mu_{\ln \delta}(t_{N_T})}{\sigma_{\ln \delta}(t_{N_T})}, \quad (2)$$

where

$$\mu_{\ln \delta}(t_{N_T}) = N_Q^{-1} \sum_{i=1}^{N_Q} \ln \delta_{q_i}(t_{N_T}), \quad (3)$$

$$\sigma_{\ln \delta}(t_{N_T})^2 = N_Q^{-1} \sum_{i=1}^{N_Q} [\ln \delta_{q_i}(t_{N_T}) - \mu_{\ln \delta}(t_{N_T})]^2, \quad (4)$$

$\delta_{q_i}(t_{N_T})$ denotes the likelihood of the most likely path ending in state q_i at step N_T , and $\delta_{q^*}(t_{N_T}) = \max_i \delta_{q_i}(t_{N_T})$ is the likelihood of the optimal path overall.

B. \mathcal{J} -statistic

The frequency domain estimator $G(f)$ converts the interferometer data into the likelihood that a signal is

TABLE I: Summary of indicative upper limits achieved in previous searches for Sco X-1. VSR2 and VSR3 are Virgo Science Runs 2 and 3, respectively. Where applicable, the upper limits refer to signals of unknown polarization.

Search	Data	Upper limit	Reference
\mathcal{F} -statistic	S2	$h_0^{95\%} \lesssim 2 \times 10^{-22}$ at 464–484 Hz, 604 – 626 Hz	[31]
\mathcal{C} -statistic	S5	$h_0^{95\%} \lesssim 8 \times 10^{-25}$ at 150 Hz	[32]
TwoSpect	S6, VSR2, VSR3	$h_0^{95\%} \lesssim 2 \times 10^{-23}$ at 20 – 57.25 Hz	[34]
Radiometer	S4, S5	$h_0^{90\%} \lesssim 2 \times 10^{-24}$ at 150 Hz	[38, 52]
TwoSpect	S6	$h_0^{95\%} \lesssim 1.8 \times 10^{-24}$ at 165 Hz	[53]
Radiometer	O1	$h_0^{90\%} \lesssim 6.7 \times 10^{-25}$ at 130 – 175 Hz	[39]
Viterbi 1.0	O1	$h_0^{95\%} \lesssim 8.3 \times 10^{-25}$ at 106 Hz	[40]
Cross correlation	O1	$h_0^{95\%} \lesssim 2.3 \times 10^{-25}$ at 175 Hz	[43]

present at frequency f . For a continuous-wave search for an isolated neutron star, the maximum-likelihood \mathcal{F} -statistic [30] is a typical choice for $G(f)$. The \mathcal{F} -statistic accounts for the diurnal rotation of the Earth, and its orbit around the Solar System barycentre. It is an almost optimal matched filter for a biaxial rotor [55].

For a neutron star in a binary system, such as an LMXB, the signal is frequency (Doppler) modulated by the binary orbital motion as well. Ref. [40] used the Bessel-weighted \mathcal{F} -statistic to account for this modulation, without using information about the orbital phase. Ref. [51] introduced the \mathcal{J} -statistic, which is a matched filter that extends the \mathcal{F} -statistic to include orbital phase in the signal model. The orbital Doppler effect distributes the \mathcal{F} -statistic power into approximately $2m+1$ orbital sidebands separated by P^{-1} , with $m = \lceil 2\pi f_* a_0 \rceil$, where $\lceil \cdot \rceil$ denotes rounding up to the nearest integer, P is the orbital period and $a_0 = (a \sin i)/c$ is the light travel time across the projected semi-major axis (where a is semi-major axis and i is the inclination angle of the binary). For a zero-eccentricity Keplerian orbit, the Jacobi-Anger identity may be used to expand the signal $h(t)$ in terms of Bessel functions, suggesting a matched filter of the form [50, 51]

$$G(f) = \mathcal{F}(f) \otimes B(f), \quad (5)$$

with

$$B(f) = \sum_{s=-m}^m J_s(2\pi f_0 a_0) e^{-is\phi_a} \delta(f - s/P), \quad (6)$$

where $J_s(z)$ is the Bessel function of the first kind of order s , ϕ_a is the orbital phase at a reference time, and δ is the Dirac delta function.

All else being equal, using the \mathcal{J} -statistic instead of the Bessel-weighted \mathcal{F} -statistic improves sensitivity by a factor of approximately four. Ref. [51], particularly Section IV of that paper, examines the difference between the two estimators in depth.

The Bessel-weighted \mathcal{F} -statistic requires a search over a_0 but does not depend on ϕ_a . By contrast, the more-sensitive \mathcal{J} -statistic involves searching over ϕ_a too. In this paper we apply the \mathcal{J} -statistic to search for Sco X-1.

Details of the search and priors derived from electromagnetic measurements are discussed in Section III.

III. LIGO O2 SEARCH

A. Sco X-1 parameters

The matched filter described in Section IIB depends on three binary orbital parameters: the period P , the projected semi-major axis a_0 and the phase ϕ_a . The \mathcal{F} -statistic depends on the sky location α (right ascension) and δ (declination), and optionally the source frequency derivatives. For this search, we assume there is no secular evolution in frequency. The other parameters have been measured electromagnetically for Sco X-1 and are presented in Table II.

For α , δ and P , the uncertainties in the electromagnetic measurements are small enough that they have no appreciable effect on the sensitivity of the search [49, 56, 57], and a single, central value can be assumed. However, the uncertainties in a_0 and ϕ_a cannot be neglected. The time spent searching orbital parameters scales as the number of (a_0, ϕ_a) pairs. Careful selection of the ranges of a_0 and ϕ_a is essential to keep computational costs low.

The previous analysis, described in Ref. [40], used the Bessel-weighted \mathcal{F} -statistic in place of the \mathcal{J} -statistic, and searched over a uniformly-gridded range of a_0 , where the grid resolution did not depend on frequency. However, the \mathcal{J} -statistic is more sensitive to mismatch in the binary orbital parameters, so a finer grid is required. We must also choose an appropriate grid for ϕ_a . (The Bessel-weighted \mathcal{F} -statistic is independent of ϕ_a .)

As the \mathcal{J} -statistic has a similar overall response to parameter mismatches as the binary \mathcal{F} -statistic, we follow the formalism in Ref. [49] to select an appropriate parameter space gridding. We choose a grid which limits the maximum loss in signal-to-noise ratio (mismatch) μ_{\max} to $\mu_{\max} = 0.1$. Equation (71) in Ref. [49] gives a general equation for the number of grid points needed for each search parameter. For the particular search considered

in this paper, the number of choices for a_0 and ϕ_a are

$$N_{a_0} = \left\lceil \frac{\pi\sqrt{2}}{2} \mu_{\max}^{-1/2} f_0 \Delta a_0 \right\rceil, \quad (7)$$

$$N_{\phi_a} = \left\lceil \frac{1}{2} \mu_{\max}^{-1/2} f_0 a_0 \left(\frac{2\pi}{P} \right) \Delta \phi_a \right\rceil, \quad (8)$$

where Δa_0 and $\Delta \phi_a$ are the widths of the search ranges for a_0 and ϕ_a respectively. The number of orbital parameters to be searched depends on the search frequency. Accordingly for each search sub-band, we adopt a different grid resolution, with the grid refined at higher frequencies. In the sub-band beginning at 60 Hz, we have $N_{a_0} = 768$ and $N_{\phi_a} = 78$; in the sub-band beginning at 650 Hz, we have $N_{a_0} = 8227$ and $N_{\phi_a} = 824$. In principle we could achieve further computational savings by noting that N_{ϕ_a} also depends on a_0 , but for safety we use the largest a_0 .

The search range for a_0 is $1.45 \leq a_0/(1\text{ s}) \leq 3.25$, which matches the most recent electromagnetic measurement [58] and widens the error bars on the widely-cited and previous best published measurement, $a_0 = 1.44 \pm 0.18\text{ s}$. [59].

The orbital phase ϕ_a can be related to the electromagnetically measured time of ascension, T_{asc} , given in Table II, by

$$\phi_a = 2\pi T_{\text{asc}}/P \pmod{2\pi}. \quad (9)$$

The one-sigma uncertainty in the published value for T_{asc} is $\pm 50\text{ s}$ [58, 60], for a time of ascension at GPS time 974 416 624 s (in November 2010). As O2 took place significantly after this time, to make a conservative estimate on appropriate error bars for T_{asc} , we advance T_{asc} by adding 3 135 orbital periods to the time of ascension taken from Ref. [58]. As there is uncertainty associated with the measured orbital period, this widens the one-sigma uncertainty of T_{asc} to $\pm 144\text{ s}$, which we round up to $\pm 150\text{ s}$. To cover a significant portion of the measured T_{asc} range while keeping the search computationally feasible, we search a two-sigma range around the central T_{asc} , namely, $1\,164\,543\,014 \leq T_{\text{asc}}/(1\text{ s}) \leq 1\,164\,543\,614$ (expressed for presentation purposes as the time of the last ascension before the start of O2).

As there is no electromagnetic measurement of f_* for Sco X-1, we search the band $60 \leq f_*/(1\text{ Hz}) \leq 650$, where LIGO is most sensitive, again adopting a uniform prior (see Section II A for a discussion of the HMM prior). The same band is analysed in Ref. [40]. For computational convenience, we split the band into blocks of approximately 0.61 Hz (discussed further in Section III B).

The final electromagnetically measured parameter is the polarization angle, ψ . Because the \mathcal{F} -statistic components of the \mathcal{J} -statistic are maximized over the polarization angle, the \mathcal{J} -statistic is insensitive to ψ .

A summary of the search ranges flowing from the electromagnetically measured parameters of Sco X-1 is presented in Table II.

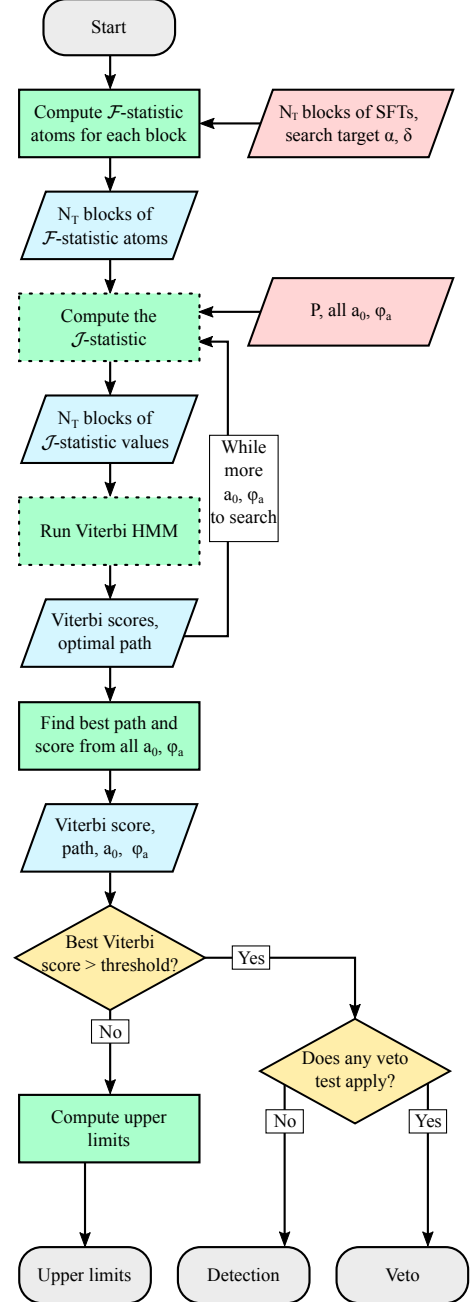


FIG. 1: Flowchart of the \mathcal{J} -statistic search pipeline for each sub-band. Note that the \mathcal{F} -statistic atoms are computed once per block and per sub-band, then the \mathcal{J} -statistic is recalculated for each (a_0, ϕ_a) pair. The grey ovals are the start and end of the algorithm, the green rectangles are procedures, the blue (red) parallelograms are intermediate (input) data, the yellow diamonds are decision points, and the grey dashed line represents a loop repeated once for each choice of parameter. The rectangles with a dashed boundary were run on graphical processing units (GPUs), while those with a solid boundary were run on central processing units (CPUs).

TABLE II: Electromagnetic measurements of the sky position and binary orbital parameters of Sco X-1. The uncertainties represent one sigma (68%) confidence intervals, except for a_0 , for which hard limits are given. The search resolution for a_0 and T_{asc} is different in each frequency sub-band, as discussed in Section III A. The search range for the time of ascension is the observed time of ascension, propagated forward to the start of O2.

Observed parameter	Symbol	Value	Reference
Right ascension	α	16 h 19 m 55.0850 s	[61]
Declination	δ	$-15^\circ 38' 24.9''$	[61]
Orbital period	P	$68\,023.86048 \pm 0.0432$ s	[58]
Projected semi-major axis	a_0	[1.45, 3.25] s	[58]
Polarisation angle	ψ	$234 \pm 3^\circ$	[62]
Orbital inclination angle	i	$44 \pm 6^\circ$	[62]
Time of ascension	T_{asc}	$974\,416\,624 \pm 50$ s	[58, 60]
Search parameter	Symbol	Search range	Resolution
Frequency	f_0	60 – 650 Hz	5.787037×10^{-7} Hz
Projected semi-major axis	a_0	1.450 – 3.250 s	variable
Time of ascension	T_{asc}	1 164 543 014 – 1 164 543 614 s	variable

B. Workflow

The workflow for the search is displayed as a flowchart in Figure 1.

The data from the detector are provided as short Fourier transforms (SFTs), each covering $T_{\text{SFT}} = 1800$ s. We divide the search into sub-bands, both to facilitate managing the volume of data, and to ensure that replacing the search frequency f with the mid-point of the sub-band, \bar{f} , is a good approximation in Equation (6). To achieve best performance from the fast Fourier transforms used to compute the convolution in (6), it is desirable to have a power of two number of frequency bins in the band, so we set the sub-band width to be $\Delta f_{\text{band}} = 2^{20} \Delta f_{\text{drift}} = 0.6068148$ Hz. This in turn sets the number of hidden states per sub-band per binary orbital parameter to be $N_Q = 2^{20}$.

For each sub-band, we divide the data into N_T blocks, each with duration $T_{\text{drift}} = 10$ d. We then compute, from the SFTs, the \mathcal{F} -statistic “atoms” [63] ($\mathcal{F}_a, \mathcal{F}_b$) for each block using the fixed parameters (α, δ, P) in Table II.

The next step is to compute the \mathcal{J} -statistic for the (a_0, ϕ_a) search grid described in Section III A. The \mathcal{F} -statistic atoms do not depend on the binary orbital parameters so they are not recomputed when calculating the \mathcal{J} -statistic. The code to compute the \mathcal{J} -statistic is based on the \mathcal{F} -statistic subroutines contained in the LIGO Scientific Collaboration (LSC) Algorithm Library (LAL) [64].

After computing the \mathcal{J} -statistic, we use the Viterbi algorithm to compute the optimal paths through the HMM trellis, i.e. the set of vectors Q^* . In principle, the tracking problem is three-dimensional (over f_0, a_0 and ϕ_a), but a_0 does not vary significantly over $T_{\text{obs}} \lesssim 1$ yr and ϕ_a varies deterministically, with the phase at timestep n given by $\phi_a(t_n) = \phi_a(t_{n-1}) + 2\pi T_{\text{drift}}/P$. Thus, it is convenient to search independently over f_0 and pairs

(a_0, ϕ_a) . This allows searches over (a_0, ϕ_a) pairs to be performed in parallel.

The result of this procedure is one log likelihood for the optimal path through the trellis terminating at every 3-tuple (f_0, a_0, ϕ_a) . Equation (2) converts these log likelihoods to Viterbi scores. As the noise power spectral density (PSD) of the detector is a function of f_0 , we compute μ and σ separately for each band. By contrast, the PSD is not a function of a_0 and ϕ_a . Therefore, we can recalculate μ and σ for every (a_0, ϕ_a) pair (rather than calculating μ and σ using every log likelihood across the entire search), thereby considerably reducing memory use. This has no significant impact on the Viterbi scores.

For each sub-band that produces a best Viterbi score lower than the detection threshold (chosen in Section III C), we compute an upper limit on the gravitational wave strain for a source in that sub-band. For Viterbi scores that exceed the threshold, we apply the veto tests described in Section IV A. We claim a detection, if a candidate survives all vetoes.

For performance reasons, the most computationally-intensive parts of the search (computing the \mathcal{J} -statistic, and the Viterbi tracking) were run using NVIDIA P100 graphical processing units (GPUs). Other steps were run using CPU codes, on Intel Xeon Gold 6140 CPUs.

C. Threshold and false alarm probability

It remains to determine a detection score threshold S_{th} corresponding to the desired false alarm probability. Consider the probability density function (PDF) $p_n(S)$ of the Viterbi score in noise. For a given threshold S_{th} and a fixed search frequency and set of binary orbital parameters, the probability that the score will exceed

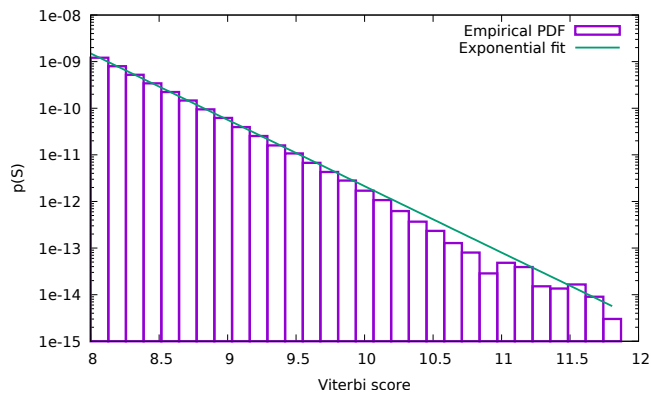


FIG. 2: Tail of the PDF of the Viterbi score S in noise. The purple histogram shows the empirical PDF derived from 10^2 realisations of the noise, analysed in the seven 0.61 Hz sub-bands starting at 55, 155, 255, 355, 455, 555 and 650 Hz. The green curve is an exponential fitted to the histogram.

this threshold (i.e. produce a false alarm) is

$$\alpha = \int_{S_{\text{th}}}^{\infty} dS p_n(S). \quad (10)$$

In general, the search covers many frequency bins and choices of binary parameters. The probability α_N of a false alarm over a search covering N parameter choices (number of frequency bins multiplied by number of binary parameter choices) is

$$\alpha_N = 1 - (1 - \alpha)^N. \quad (11)$$

This equation assumes that the Viterbi score in noise is an independent random variable at each point in the parameter space, which is not necessarily true, as the \mathcal{J} -statistic calculated for two points nearby in parameter space are correlated to some degree. However, for $\mu_{\text{max}} = 0.1$ as used in this search, these correlations do not have a significant impact [65]. In practice, we fix α_N and N and solve (10) and (11) for α and hence S_{th} .

As the noise-only PDF $p_n(S)$ of the Viterbi score is unknown analytically [40], we resort to Monte-Carlo simulations. We generate 10^2 Gaussian noise realisations in seven sub-bands of width Δf_{band} , namely those starting at 55 Hz, 155 Hz, 255 Hz, 355 Hz, 455 Hz, 555 Hz and 650 Hz. The noise is generated using the standard LIGO tool *lalapps.Makefakedata.v4*. These are the same sub-bands used in Section IIIC of Ref. [40], and the one-sided noise PSD $S_h(f)$ is set to match the O2 data. We then perform the search described in Section IIIB (including scanning over a_0 and ϕ_a).

The results of this search produce an empirical version of $p_n(S)$. Plotting the tail of this distribution on a logarithmic plot suggests that a fit to a function of the form $e^{\lambda S}$ is an appropriate choice to allow the PDF to be extrapolated in order to solve (11).

TABLE III: Results of investigating the empirical PDF of the Viterbi score in seven sub-bands in Gaussian noise. The second column is λ obtained by fitting the PDF to $e^{\lambda S}$. The third column is the threshold S_{th} obtained by solving equation (11).

Start of band (Hz)	λ	S_{th}
55	-3.02	14.12
155	-3.24	13.63
255	-3.26	13.58
355	-3.27	13.61
455	-3.30	13.62
555	-3.29	13.66
650	-3.29	13.63

We first analyse each band independently, to ensure that there is no frequency dependence in $p_n(S)$. Table III gives the best-fit λ , and the threshold S_{th} obtained, for each band analysed in isolation. We find that there is no significant dependence on the sub-band searched, nor any identifiable trend in λ or S_{th} . Combining the realisations for all bands produces $\lambda = -3.28$ and hence $S_{\text{th}} = 13.66$ for $\alpha = 0.01$. The empirical PDF and fitted exponential are shown in Figure 2.

D. Sensitivity

After selecting S_{th} , it remains to determine the lowest (as a function of frequency) characteristic wave strain, $h_0^{95\%}$, that can be detected with 95 per cent efficiency (i.e., a five per cent false dismissal rate). To do this, we generate Monte-Carlo realisations of Gaussian noise with Sco X-1-like signals injected. We determine the proportion of signals recovered as a function of h_0 and double-check the false alarm probability quoted above.

For O2, the most sensitive sub-band of width $\Delta f_{\text{band}} = 0.6068148$ Hz is the one beginning at 194.6 Hz. Following a typical procedure used to find upper limits for continuous gravitational wave searches [66], we generate 10^2 noise realisations and inject signals, using the source parameters in Table II, with $T_{\text{obs}} = 230$ d (the duration of O2), $T_{\text{drift}} = 10$ d, $N_T = 23$, $\sqrt{S_h} = 7.058 \times 10^{-24} \text{Hz}^{-1/2}$, and $\cos \iota = 1$. The remaining range-bound parameters, namely $f_{0\text{inj}}$, $a_{0\text{inj}}$, T_{ascinj} and ψ_{inj} are chosen from a uniform distribution within the range given by their $1\text{-}\sigma$ error bars. The source frequency $f_{0\text{inj}}$ is chosen from a uniform distribution on the interval [194.6 Hz, 194.7 Hz]. For each realisation, the signal is injected with progressively lower h_0 until it can no longer be detected. We denote by $h_{0,\text{min};i}$ the lowest h_0 that can be detected in realisation i . To obtain $h_0^{95\%}$, we take the 95th highest $h_{0,\text{min};i}$. The simulations return the threshold $h_0^{95\%} = 1.46 \times 10^{-25}$ at 194.6 Hz.

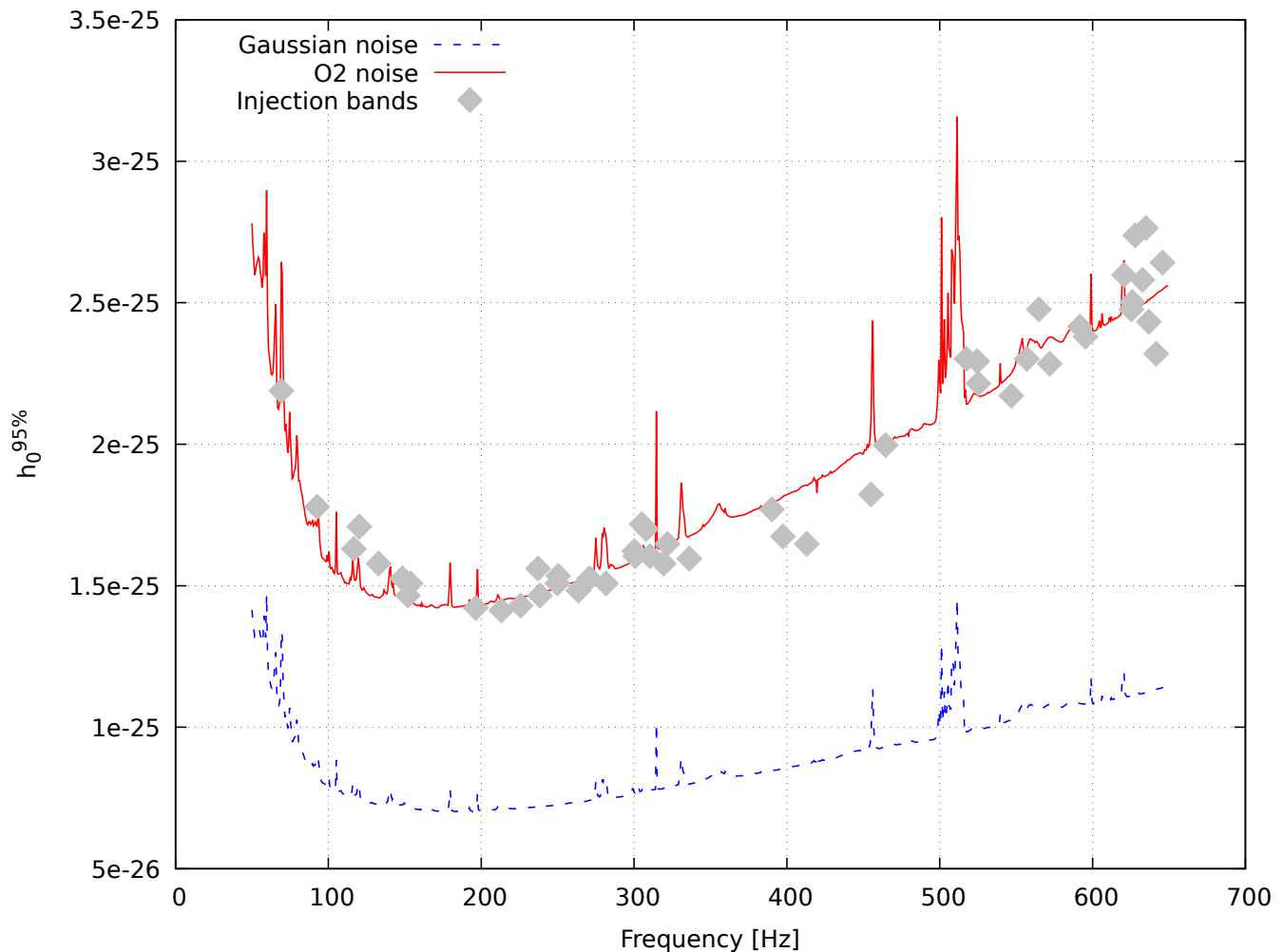


FIG. 3: Sensitivity of a search for Sco X-1, across the frequency band searched in this work. The horizontal axis shows the search frequency. The vertical axis shows the wave strain $h_0^{95\%}$ needed for a 95% detection efficiency, on the assumption $\cos \iota = 1$, namely, a circularly polarized signal. The blue dashed curve is based on simulations of Gaussian noise, while the red solid curve is corrected for the non-Gaussian statistics of the noise and the interferometer duty cycle, through multiplying by $\kappa_{\text{freq}}(f)$ (see Section III D). The diamonds show $h_0^{95\%}$ derived through injections into sub-bands, again assuming a circularly polarized signal (see Section III D).

In general, the signal-to-noise ratio is strongly affected by the inclination angle ι , not just h_0 . We follow Ref. [60] and define an effective h_0 that absorbs the dependence on ι :

$$h_0^{\text{eff}} = h_0 2^{-1/2} \{[(1 + \cos^2 \iota)/2]^2 + \cos^2 \iota\}^{1/2}, \quad (12)$$

allowing us to generalize results from the simulations above, where all injections were done with $\cos \iota = 1$. Thus, the result obtained above corresponds to circular polarization. The electromagnetically measured inclination of Sco X-1's orbit is $i \approx 44^\circ \pm 6^\circ$ [62]. Although it is not necessarily the case, if we assume that the orbital inclination equals the inclination angle ι of the putative neutron star's spin axis, we obtain $h_0^{\iota \approx 44^\circ, 95\%} = 1.35 h_0^{\text{eff}, 95\%}$.

The search in Ref. [40] found a scaling relation of the

form $h_0^{95\%} \propto S_h^{1/2} f_0^{1/4}$, to hold for fixed T_{obs} . The $f_0^{1/4}$ dependence arises because the latter search added sidebands incoherently. In the case of the \mathcal{J} -statistic, which adds sidebands coherently, we expect the scaling to depend just on h_0 , with

$$h_0^{95\%} \propto S_h^{1/2}. \quad (13)$$

We verify this scaling in Gaussian noise by repeating the injection procedure described above in frequency bands beginning at 55 Hz, 355 Hz and 650 Hz. The scaling is the final ingredient needed to produce the blue dashed curve in Figure 3, which shows the expected sensitivity of a search over the full search band, assuming Gaussian noise, a 100 per cent duty cycle and a circularly polarized signal.

There is no simple scaling similar to (13) that can be

used to account for the effect of non-Gaussian noise and the detector duty cycle. Hence we introduce a multiplicative correction factor κ_j for a selection of sub-bands indexed by j , following Ref. [40]. We determine κ_j by doing 10^2 injections (drawing parameters as described above) into the detector data for the j -th sub-band, again using progressively-lower h_0 until we determine the minimum h_0 detected. Then, κ_j equals $h_0^{\text{eff},95\%}$ for injections into real noise, divided by $h_0^{\text{eff},95\%}$ for injections into Gaussian noise.

Producing κ_j in this way for a random selection of sub-bands in the search band suggests that κ depends weakly on frequency, most likely due to the \mathcal{J} -statistic not perfectly summing sidebands [40]. A linear fit to the computed κ_j values suggests a frequency-dependent correction factor

$$\kappa_{\text{freq}}(f) = 1.944 + 4.60 \times 10^{-4} f / (1 \text{ Hz}). \quad (14)$$

We use $\kappa_{\text{freq}}(f)$ to adjust the blue dashed curve in Figure 3, producing the red solid curve in that figure, which represents the expected sensitivity across the full search band, where the noise is realistic (i.e. not Gaussian). The 50 sub-bands sampled are shown on the plot as grey diamonds.

IV. O2 ANALYSIS

We now analyse the data from LIGO’s Observing Run 2 (O2), using the full dataset from 30 November 2016 to 26 August 2017, including data from the LIGO Livingston (L1) and Hanford (H1) observatories. The Virgo interferometer also participated in the last two months of O2, but we do not use any Virgo data in this analysis.

There are two notable pauses in data gathering: an end-of-year break starting on 22 December 2016 lasting for 13 days, and a commissioning break starting on 7 May 2017 lasting for 19 (L1) or 32 (H1) days.

Data stretches shorter than T_{SFT} are discarded, as is a period of approximately one month where much of the band was contaminated, due to a blinking light in the power system and a digital camera (used for detector diagnostics) that was inadvertently left on. A detailed discussion of Advanced LIGO detector noise can be found in Ref. [67]. Taking all these factors into account, the overall duty cycle (i.e. proportion of time spent gathering science-quality data) for O2 was 51.9% (L1) and 46.2% (H1).

Because of the commissioning break, one ten-day block has no data. We fill this block with uniform log likelihood, so that the HMM has no preference for remaining in the same frequency bin, or moving by one bin, during the break, while still allowing a maximum drift of Δf_{drift} every ten days. An alternative, but equivalent, approach would be to remove the break entirely, and alter the transition matrix $A_{q_i q_j}$ for that step to allow the HMM to wander up to two frequency bins. The end-of-year break is also longer than ten days, but it is covered

by two blocks. Both of the blocks that overlap with the end-of-year break contain data.

We search the same frequency band as Ref. [40], namely 60 – 650 Hz. The lower limit is set by LIGO’s poor sensitivity for signals $\lesssim 25$ Hz and the significant contamination from instrumental noise in the band 25 – 60 Hz. The sensitivity of the search falls as frequency increases, while compute time rises dramatically. We terminate the search at 650 Hz, as in Ref. [40].

The results of the search are presented in Figure 4, which shows the frequency and recovered orbital parameters a_0 and ϕ_a for every path with $S > S_{\text{th}}$. The colour of the points shows the Viterbi score associated with that path. As the most a signal can wander during the observation is $N_T \Delta f_{\text{drift}} \approx 1.3 \times 10^{-5}$ Hz, which is small compared to Δf_{band} (and what can be visually discerned on Figure 4), we define f_0 for a given path to be equal to $f_0(t = N_T)$ for convenience.

To rule out false alarms, we apply the hierarchy of vetoes first described in Ref. [40]. The vetoes are: (1) the known instrumental lines veto (described in Section IV A 1 below), (2) the single interferometer veto (Section IV A 2), (3) the $T_{\text{obs}}/2$ veto (Section IV A 3) and (4) the T_{drift} veto (ultimately not used, but discussed in Section IV A 4 of Ref. [40]). To ensure that the vetoes are unlikely to falsely dismiss a true signal, we perform the search on a dataset with synthetic signals injected into it, and ensure that those injections are not vetoed. These veto safety tests are described in Section IV B.

The number of candidates found in the initial search, and then vetoed at each step, are listed in Table V.

A. Vetoes

1. Known lines veto

There are a large number of persistent instrumental noise lines identified as part of LIGO’s detector characterisation process [67, 68]. These lines can arise from a number of sources, including interference from equipment around the detector, resonant modes in the suspension system, and external environmental causes (e.g. the electricity grid).

A noise line generally produces high $|\mathcal{F}_a|$ and $|\mathcal{F}_b|$ values. The convolution in (6) reduces the impact of this somewhat by summing bins near and far from the line, but in practice the noise lines are strong enough that they contaminate any candidate nearby. Accordingly, we veto any candidate whose Viterbi path $f_0(t)$ satisfies $|f_0(t) - f_{\text{line}}| < 2\pi a_0 f_0 / P$, for any time t along the path and for any line frequency f_{line} . This veto is efficient, excluding 14 of the 20 candidates.

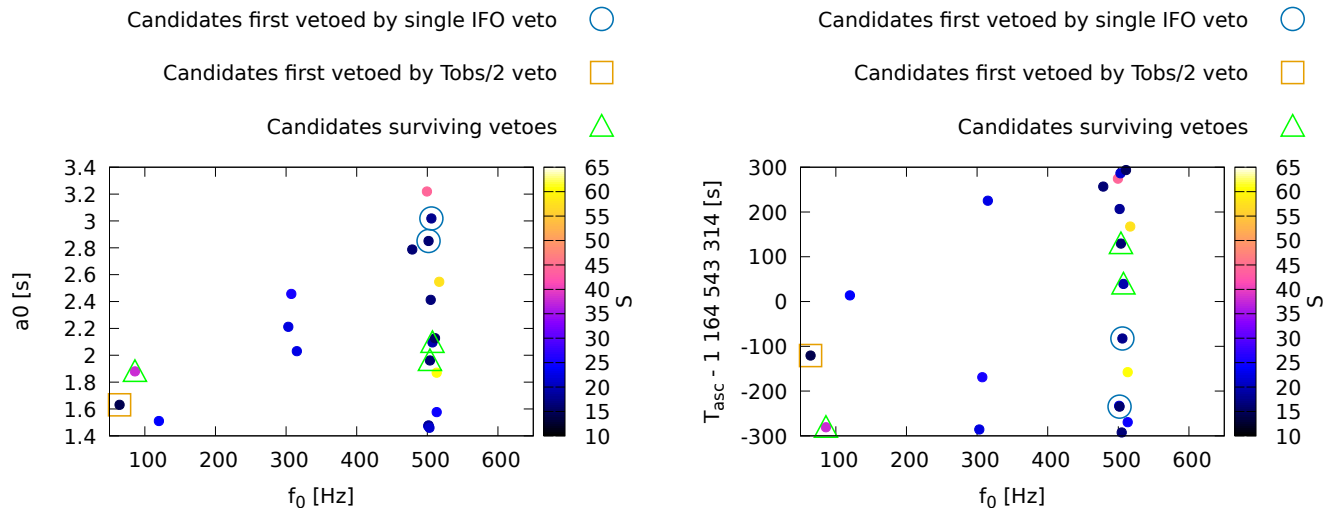


FIG. 4: Candidates identified by the search. The left hand panel plots the detection score S (indicated by colour; see colour bar) as a function of final frequency $f_0(t_{N_T})$ (horizontal axis) and orbital semi-major axis a_0 (vertical axis) recovered by the HMM. The right hand panel plots the candidates with T_{asc} on the vertical axis. Undecorated candidates are eliminated by the known line veto, candidates marked by blue circles are eliminated by the single interferometer veto, candidates marked by orange squares are eliminated by the $T_{\text{obs}}/2$ veto, and the candidates marked by green triangle survive the veto process.

2. Single interferometer veto

During O2, L1 was slightly more sensitive than H1, but overall the sensitivities of the two interferometers were similar. Accordingly, any astrophysical signal that can be detected in the combined dataset should either be detected by the individual detector datasets when analysed separately (for stronger signals) or in neither (for weaker signals). A signal that is detectable in one interferometer only is likely to be a noise artifact, so we veto it.

Following Ref. [40], we compare the Viterbi scores obtained from individual detectors to the original combined score S_U to classify survivors of the known line veto into four categories, discussed below, one of which is vetoed.

Category A. One detector returns $S < S_{\text{th}}$, while the other detector returns $S > S_U$, and the frequency estimated by the latter detector is close to that of the original candidate f_{0U} , that is, $|f_{0U} - f_0| < 2\pi a_{0U} f_{0U}/P$, where the subscript U denotes a quantity estimated by the search in both detectors. This category, and the next, represent signals where the score is dominated by one detector. We veto candidates in Category A.

Category B. As with Category A, one detector returns $S < S_{\text{th}}$, while the other detector returns $S > S_U$. Unlike Category A, the frequency estimated by the latter detector is far from the original candidate, i.e., $|f_{0U} - f_0| > 2\pi a_{0U} f_{0U}/P$. In this case, it is possible that there is signal at f_{0U} which is detectable when combining the data from both detectors but not from one detector, because some artifact masks its presence. Hence we keep the candidate for follow-up.

Category C. The candidate is seen with $S > S_{\text{th}}$ in both detectors. This could either be a relatively strong signal, or an artifact from a noise source common to both detectors. The single interferometer veto cannot distinguish these possibilities. Again, we keep the candidate for follow-up.

Category D. The candidate is not seen by either detector, with $S < S_{\text{th}}$ in both detectors. This could be a signal that is too weak to see in either detector individually. We keep the candidate for follow-up.

Category A of the single-interferometer veto eliminates two of the remaining six candidates. The two eliminated candidates were stronger in H1 compared to L1.

3. $T_{\text{obs}}/2$ veto

We divide the observing run into two segments, the first covering 140 days from 30 Nov 2016 (GPS timestamp 1 164 562 334) to 19 Apr 2017 (GPS timestamp 1 176 658 334), and the second covering 90 days from 19 Jan 2017 (GPS timestamp 1 168 882 334) to 25 Aug 2017 (GPS timestamp 1 187 731 792). This division is chosen to get approximately equal effective observing time in the two segments. There is no forceful evidence to suggest that the gravitational wave strength of an LMXB varies significantly with time (and a signal with time-varying strength is likely to have a considerably more complicated form than assumed here); thus we do not expect a signal to appear preferentially in either segment. We search the segments separately for the candidates which

survived both preceding vetoes. To determine whether to veto candidates at this stage, we apply the same set of categories as in veto 2.

This veto eliminates one remaining candidate, which is much stronger in the first segment of the observing run than the second.

Ref. [40] describes the T_{drift} veto as a fourth veto that can be applied to candidates surviving the $T_{\text{obs}}/2$ veto. However, this veto is applicable to candidates with an observed spin wandering timescale that is 20 days or longer. This is not the case for the surviving three candidates, so the T_{drift} veto is not applicable to them.

The remaining candidates are in the sub-bands starting at 85.4 Hz, 503.6 Hz and 507.2 Hz. The scores relevant to performing the veto procedure are given in Table IV. All three candidates are stronger when analyzing the H1 detector data alone compared to analyzing L1 detector data alone, with the L1 results consistent with noise. The candidates in the sub-bands starting at 85.4 Hz and 507.2 Hz are both stronger during the second half of O2 compared to the first half, while the candidate in the sub-band starting at 503.6 Hz is stronger in the analysis of the first half of O2. Particularly for the candidate in the 85.4 Hz sub-band, the asymmetry in score between the first and second half of the observing is extreme and suggestive of a detector artifact rather than an astrophysical signal. The asymmetry is less pronounced for the candidates in the sub-bands starting at 503.6 Hz and 507.2 Hz, but both of these candidates are in a region of frequency space that is significantly contaminated by interferometer noise, particularly violin modes associated with the LIGO mirror suspension. For these reasons, it is most likely that these candidates are due to unknown instrumental noise in the H1 detector, although they are not formally ruled out by the veto procedure described above.

B. Veto safety

To verify that the vetoes described previously do not unduly increase the false dismissal probability, we inject signals into the O2 data and perform the veto procedure described in the previous section. We inject a total of 50 signals into 50 sub-bands of width Δf_{band} , chosen to be comparable to the 200 injections used for the equivalent tests in Ref. [40] while having a large enough sample to be confident that false dismissals caused by the vetoes are rare in the context of the five per cent false dismissal rate used in calculating sensitivity. The sub-bands and parameters chosen are selected randomly from the search band to achieve good frequency coverage, but excluding those sub-bands that contain a known line (and hence would be excluded by the known lines veto). Into these sub-bands, we inject a signal near the detection limit with h_0 typically at $h_0^{95\%}$ for that sub-band (although we inject a stronger signal if the signal turns out to be undetectable), and with f_0 drawn randomly from a uniform distribution over the

interval $[f_{\text{start}} + 0.1 \text{ Hz}, f_{\text{start}} + \Delta f_{\text{band}} - 0.1 \text{ Hz}]$, where f_{start} is the lowest frequency in the sub-band. At each block, the signal is allowed to wander at most one frequency bin (i.e., by an amount drawn uniformly from $[-\Delta f_{\text{drift}}, +\Delta f_{\text{drift}}]$), and the signal frequency is constant within the block, following Ref. [40]. The other parameters chosen in the same way as for the sensitivity tests described in Section III D.

We then apply vetoes 2 (single interferometer veto) and 3 ($T_{\text{obs}}/2$ veto) to each candidate (veto 1 is inapplicable, as the injection bands avoid known lines; and veto 4 [T_{drift} veto] was not used in this search). No injection was vetoed.

Because the veto safety procedure uses the O2 data as noise, it is possible that the safety results described above depend in some way on the specifics of O2. However, as the veto procedure copies the equivalent procedure in Ref. [40], which tests both S5 noise and O1 noise, we have confidence that the veto safety result is not specific to the peculiarities of O2.

V. UPPER LIMITS

We can use the non-detection reported in the previous section, in concert with the approach outlined in Section III D, to place an upper limit on h_0 as a function of f_0 and compare the result to the indirect, torque-balance upper limit established by the X-ray flux [20].

A. Frequentist upper limit at 95% confidence

Failure to detect a gravitational wave signal allows us to place an upper limit on h_0 from a particular source, given a desired confidence level. In this section, we follow Ref. [40] in using a frequentist approach and setting 95% as the desired confidence level. The alternative, Bayesian approach in Ref. [57] is hard to adapt to the HMM-based search, because correlations between the Viterbi paths render the distribution of Viterbi scores difficult to calculate analytically.

We define $h_0^{95\%}$ to be the lowest amplitude signal for which we have a 95% probability or greater of detecting a signal with $h_0 \geq h_0^{95\%}$, that is, $\Pr(S \geq S_{\text{th}} | h_0 \geq h_0^{95\%}) \geq 0.95$. The value of $h_0^{95\%}$ depends on the inclination angle of the source, through equation (12). Figure 5 show the upper limit for three cases: assuming the neutron star spin axis inclination angle ι is equal to the electromagnetically-constrained orbital inclination angle $i \approx 44^\circ$ (purple plus signs), a pure circularly-polarized signal $|\cos \iota| = 1$ (green crosses), and a flat prior on $\cos \iota$ (blue asterisks). For sub-bands with no candidate path with a Viterbi score above the threshold, we take $h_0^{95\%}$ from Figure 3 for the circularly-polarized case, and determine $h_0^{95\%}$ for the two other cases using equation (12). No upper limit is established for sub-bands containing a vetoed candidate (because those bands are deemed to

TABLE IV: Viterbi scores of the three candidates that survived the veto procedure. The original score is the score of the original candidate, from the search on the full O2 dataset. The H1 and L1 scores are the scores for the candidate when searching on each detector independently. The first and second part scores are the scores when analyzing the first 140 and last 90 days of the dataset, respectively.

Sub-band containing candidate	Original score	H1	L1	First part	Second part
85.4	42.4	30.7	6.3	7.2	41.8
503.6	41.3	34.6	5.8	37.5	6.1
507.2	17.3	10.6	6.1	10.2	16.4

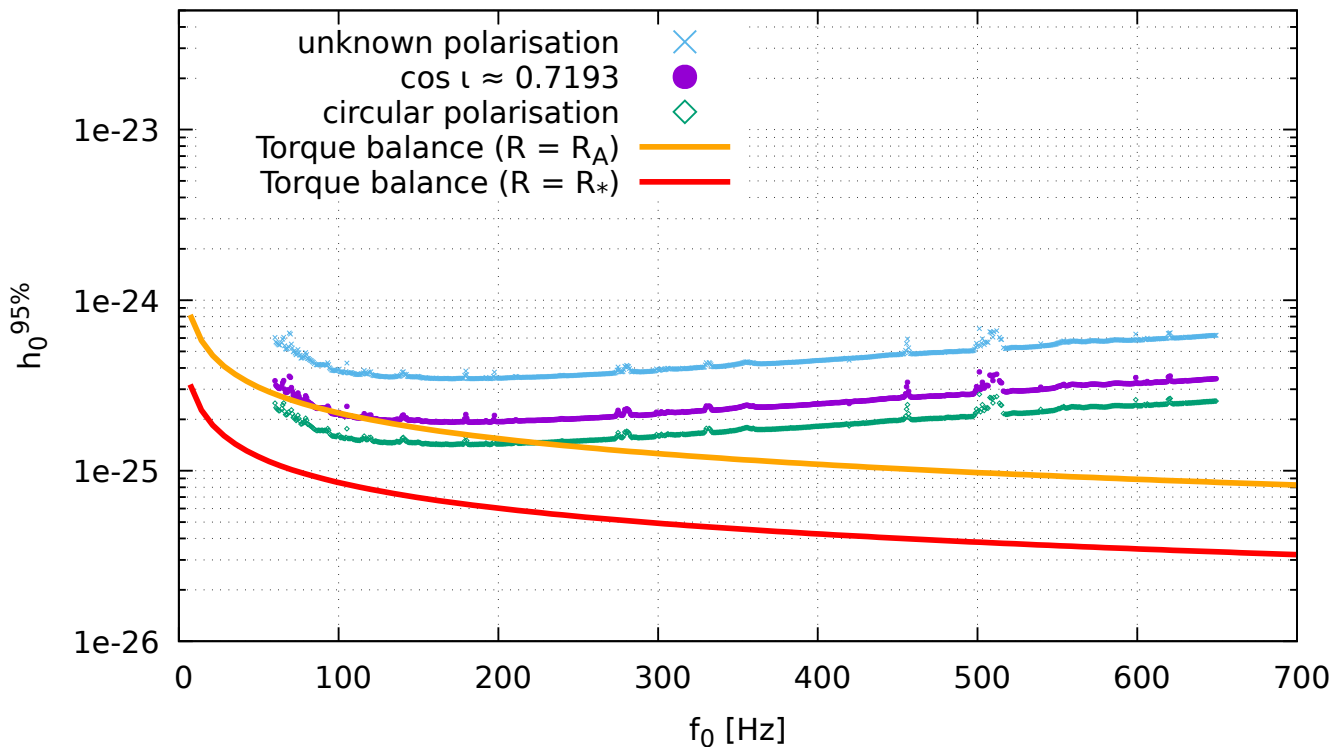


FIG. 5: Wave strain upper limits at 95% confidence as a function of signal frequency, corresponding to the frequentist upper limit in each sub-band (width Δf_{band}), for three scenarios: a flat prior on $\cos \iota$ (blue crosses), the orientation $\iota \approx 44^\circ$ derived from observations of the radio jet (filled purple circles) and the most optimistic case of circularly polarized waves (open green diamonds). These are compared to the indirect torque-balance upper limit, where the accretion torque is applied at the Alfvén radius (solid orange curve) or the stellar radius (solid red curve).

TABLE V: Number of candidates found in the first pass, and number remaining after applying the vetoes described in Section IV A.

After veto	Survivors
First pass	20
Line	6
Single interferometer	4
$T_{\text{obs}}/2$	3

be contaminated by instrumental artifacts). Accordingly those sub-bands are excluded from Figure 5.

The circularly-polarized case produces the most stringent upper limit, reflecting the fact that $|\cos \iota| = 1$ would be the most favourable configuration for producing gravitational waves. Conversely, assuming no knowledge of the inclination angle (the flat prior case) produces a looser upper limit. The lowest upper limit for this search is in the sub-band starting at 194.6 Hz, with upper limits of $h_0^{95\%} = 3.47 \times 10^{-25}$, 1.93×10^{-25} , 1.42×10^{-25} for the unknown polarization, electromagnetically constrained, and circularly polarized cases, respectively. Previous work with the HMM, in Ref. [40], found $h_0^{95\%} = 8.3 \times 10^{-25}$, 4.0×10^{-25} , 3.0×10^{-25} for those cases in its most sensitive sub-band, starting at 106

Hz.

B. Torque-balance upper limit

An indirect upper limit on gravitational wave strain can be obtained from X-ray observations. If the spin-down torque due to gravitational wave emission balances the accretion spin-up torque, with the latter inferred from the X-ray luminosity, one has $h_0 \geq h_0^{\text{eq}}$ with [20, 22, 56]

$$h_0^{\text{eq}} = 5.5 \times 10^{-27} \left(\frac{F_X}{10^{-8} \text{ erg cm}^{-1} \text{ s}^{-1}} \right)^{1/2} \left(\frac{R}{10 \text{ km}} \right)^{3/4} \left(\frac{1.4M_\odot}{M_\star} \right)^{1/4} \left(\frac{300 \text{ Hz}}{f_\star} \right)^{1/2}, \quad (15)$$

where F_X is the X-ray flux, R is the length of the notional “lever arm” to which the accretion torque is applied, M_\star is the stellar mass and f_\star is the (unknown) spin frequency.

To establish an upper limit, we take the electromagnetically measured $F_X = 4 \times 10^{-7} \text{ erg cm}^{-2} \text{ s}^{-1}$ [47] of Sco X-1, and the common fiducial neutron star mass $M_\star = 1.4M_\odot$. The most conservative choice for the accretion torque lever arm is the stellar radius $R_\star = 10 \text{ km}$. We plot h_0^{eq} as a function of frequency as the solid red curve in Figure 5. Another physically reasonable choice of lever arm length is the Alfvén radius, R_A , i.e. the distance out to which outflowing material co-rotates with the star’s magnetic field. This is given by [40, 46]

$$R_A = 35 \left(\frac{B_\star}{10^9 \text{ G}} \right)^{4/7} \left(\frac{R_\star}{10 \text{ km}} \right)^{12/7} \left(\frac{1.4M_\odot}{M_\star} \right)^{1/7} \left(\frac{10^{-8} M_\odot \text{ yr}^{-1}}{\dot{M}} \right)^{2/7} \text{ km}, \quad (16)$$

where B_\star is the polar magnetic field strength at the stellar surface, G is Newton’s gravitational constant and \dot{M} is the accretion rate. The accretion rates in LMXBs can range from the Eddington limit, $2 \times 10^{-8} M_\odot \text{ yr}^{-1}$, down to about $10^{-11} M_\odot \text{ yr}^{-1}$ [69, 70]. The magnetic fields on the neutron stars in LMXBs are comparatively weak, lying in the range $10^8 \text{ G} \lesssim B_\star \lesssim 10^9 \text{ G}$ [20, 70, 71]. We substitute $\dot{M} = 10^{-8} M_\odot \text{ yr}^{-1}$ and $B_\star = 10^9 \text{ G}$ into equation (16), to maximize R_A and hence h_0^{eq} . The result is plotted as the orange curve in Figure 5. Both torque balance curves are plotted with $f_0 = 2f_\star$, i.e. an orthogonal biaxial rotor, which is a conventional assumption [30].

At the most sensitive sub-band, starting at $f_0 = 194.6 \text{ Hz}$, the electromagnetically-constrained upper limit is a factor of about 1.2 below (3.1 above) the torque balance for $R = R_A$ ($R = R_\star$). The upper limits for a circularly-polarized signal beat the $R = R_A$ torque balance upper limit between 60 and 223 Hz; and the upper limits assuming an electromagnetically constrained inclination angle beat the $R = R_A$ torque balance limit between 94 Hz and 113 Hz.

The upper limits given in Figure 5 are somewhat higher than those achieved by the most sensitive search to date, the O1 cross-correlation search, which has upper limits that are typically lower by a factor of approximately 1.5 [43]. A significant contributing factor to this is that the threshold S_{th} is set by assuming that the search at each binary orbital parameter is independent, while in fact there are significant correlations between adjacent points in search parameter space. These correlations are difficult to safely account for and so we make the conservative assumption that they are independent. Thus S_{th} is an overestimate of the threshold for a one per cent false alarm probability, in turn overestimating the upper limits and making a direct comparison of the upper limits difficult.

This search also uses updated binary orbital parameter ranges, taking advantage of a more recent analysis of electromagnetic observations to produce a search better targeted at Sco X-1. Similarly, while the detector design is fundamentally unchanged between O1 and O2, various detector improvements mean that some instrumental lines have been removed or ameliorated, making this search sensitive to signals that would have been obscured by instrumental noise in searches using earlier datasets. The hidden Markov model is also designed with particular emphasis on robustness to spin wandering. Together, these three reasons mean that the search covers a slightly different region of parameter space compared to previous Sco X-1 searches.

VI. CONCLUSION

In this paper, we search the LIGO O2 dataset for continuous gravitational waves from the LMXB Sco X-1, using a hidden Markov model combined with the \mathcal{J} -statistic. We find no signal. The search band extends from 60 Hz to 650 Hz. The sky location α , δ and orbital parameters P , a_0 and ϕ_a used for the matched filter are electromagnetically constrained; values are given in Table II. Monte-Carlo simulations of spin-wandering signals injected into the LIGO O2 data imply frequentist 95% upper limits of $h_0^{95\%} = 3.47 \times 10^{-25}$, 1.92×10^{-25} , 1.42×10^{-25} for unknown, electromagnetically restricted ($\cos \iota \approx 0.72$) and circular polarizations respectively. The upper limits apply at 194.6 Hz, which is the most sensitive search frequency. For the electromagnetically-restricted case, the limit is 3.1 times above, or 1.2 times below, the torque-balance limit, when the torque-balance lever arm is the stellar radius or the Alfvén radius respectively. Monte-Carlo simulations are used to establish a detection threshold corresponding to a false alarm probability of $\alpha = 0.01$.

These results improve on the results from the previous HMM search, described in Ref. [40], by using data from LIGO’s second observing run, and by substituting the \mathcal{J} -statistic for the Bessel-weighted \mathcal{F} -statistic to track the phase of the orbital Doppler shift. As a result, the

search in this paper is ≈ 2 times more sensitive compared to that in Ref.[40]. The analysis remains computationally efficient, requiring $\lesssim 3 \times 10^5$ GPU-hr for the search itself and $\lesssim 10^6$ GPU-hr for simulations to characterize the sensitivity and false alarm rate.

VII. ACKNOWLEDGEMENTS

The authors gratefully acknowledge the support of the United States National Science Foundation (NSF) for the construction and operation of the LIGO Laboratory and Advanced LIGO as well as the Science and Technology Facilities Council (STFC) of the United Kingdom, the Max-Planck-Society (MPS), and the State of Niedersachsen/Germany for support of the construction of Advanced LIGO and construction and operation of the GEO600 detector. Additional support for Advanced LIGO was provided by the Australian Research Council. The authors gratefully acknowledge the Italian Istituto Nazionale di Fisica Nucleare (INFN), the French Centre National de la Recherche Scientifique (CNRS) and the Foundation for Fundamental Research on Matter supported by the Netherlands Organisation for Scientific Research, for the construction and operation of the Virgo detector and the creation and support of the EGO consortium. The authors also gratefully acknowledge research support from these agencies as well as by the Council of Scientific and Industrial Research of India, the Department of Science and Technology, India, the Science & Engineering Research Board (SERB), India, the Ministry of Human Resource Development, India, the Spanish Agencia Estatal de Investigación, the Vicepresidència

i Conselleria d’Innovació, Recerca i Turisme and the Conselleria d’Educació i Universitat del Govern de les Illes Balears, the Conselleria d’Educació, Investigació, Cultura i Esport de la Generalitat Valenciana, the National Science Centre of Poland, the Swiss National Science Foundation (SNSF), the Russian Foundation for Basic Research, the Russian Science Foundation, the European Commission, the European Regional Development Funds (ERDF), the Royal Society, the Scottish Funding Council, the Scottish Universities Physics Alliance, the Hungarian Scientific Research Fund (OTKA), the Lyon Institute of Origins (LIO), the Paris Île-de-France Region, the National Research, Development and Innovation Office Hungary (NKFIH), the National Research Foundation of Korea, Industry Canada and the Province of Ontario through the Ministry of Economic Development and Innovation, the Natural Science and Engineering Research Council Canada, the Canadian Institute for Advanced Research, the Brazilian Ministry of Science, Technology, Innovations, and Communications, the International Center for Theoretical Physics South American Institute for Fundamental Research (ICTP-SAIFR), the Research Grants Council of Hong Kong, the National Natural Science Foundation of China (NSFC), the Leverhulme Trust, the Research Corporation, the Ministry of Science and Technology (MOST), Taiwan and the Kavli Foundation. The authors gratefully acknowledge the support of the NSF, STFC, INFN, CNRS, Swinburne University of Technology, the National Collaborative Research Infrastructure Strategy of Australia, and the State of Niedersachsen/Germany for provision of computational resources.

This work has been assigned LIGO document number ligo-p1800208.

-
- [1] K. Riles, *Progress in Particle and Nuclear Physics* **68**, 1 (2013).
 - [2] G. M. Harry and LIGO Scientific Collaboration, *Classical and Quantum Gravity* **27**, 084006 (2010).
 - [3] LIGO Scientific Collaboration, J. Aasi, B. P. Abbott, R. Abbott, T. Abbott, M. R. Abernathy, K. Ackley, C. Adams, T. Adams, P. Addesso, and et al., *Classical and Quantum Gravity* **32**, 074001 (2015), arXiv:1411.4547 [gr-qc].
 - [4] F. Acernese *et al.* (VIRGO), *Class. Quant. Grav.* **32**, 024001 (2015), arXiv:1408.3978 [gr-qc].
 - [5] N. Andersson, V. Ferrari, D. I. Jones, K. D. Kokkotas, B. Krishnan, J. S. Read, L. Rezzolla, and B. Zink, *General Relativity and Gravitation* **43**, 409 (2011), arXiv:0912.0384 [astro-ph.SR].
 - [6] G. Ushomirsky, C. Cutler, and L. Bildsten, *MNRAS* **319**, 902 (2000).
 - [7] N. K. Johnson-McDaniel and B. J. Owen, *Phys. Rev. D* **88**, 044004 (2013), arXiv:1208.5227 [astro-ph.SR].
 - [8] C. Cutler, *Phys. Rev. D* **66**, 084025 (2002), gr-qc/0206051.
 - [9] A. Mastrano, A. Melatos, A. Reisenegger, and T. Akgün, *MNRAS* **417**, 2288 (2011), arXiv:1108.0219 [astro-ph.HE].
 - [10] P. D. Lasky and A. Melatos, *Phys. Rev. D* **88**, 103005 (2013), arXiv:1310.7633 [astro-ph.HE].
 - [11] J. S. Heyl, *ApJ* **574**, L57 (2002).
 - [12] P. Arras, E. E. Flanagan, S. M. Morsink, A. K. Schenk, S. A. Teukolsky, and I. Wasserman, *ApJ* **591**, 1129 (2003), astro-ph/0202345.
 - [13] R. Bondarescu, S. A. Teukolsky, and I. Wasserman, *Phys. Rev. D* **79**, 104003 (2009), arXiv:0809.3448.
 - [14] C. Peralta, A. Melatos, M. Giacobello, and A. Ooi, *ApJ* **644**, L53 (2006), gr-qc/0604123.
 - [15] C. A. van Eysden and A. Melatos, *Classical and Quantum Gravity* **25**, 225020 (2008), arXiv:0809.4352 [gr-qc].
 - [16] M. F. Bennett, C. A. van Eysden, and A. Melatos, *MNRAS* **409**, 1705 (2010), arXiv:1008.0236 [astro-ph.SR].
 - [17] A. Melatos, J. A. Douglass, and T. P. Simula, *ApJ* **807**, 132 (2015).
 - [18] D. Chakrabarty, E. H. Morgan, M. P. Muno, D. K. Galloy, R. Wijanands, M. van der Klis, and C. B. Markwardt, *Nature* **424**, 42 (2003), astro-ph/0307029.
 - [19] G. B. Cook, S. L. Shapiro, and S. A. Teukolsky, *ApJ*

- 424**, 823 (1994).
- [20] L. Bildsten, *The Astrophysical Journal Letters* **501**, L89 (1998), astro-ph/9804325.
- [21] J. Papaloizou and J. E. Pringle, *MNRAS* **184**, 501 (1978).
- [22] R. V. Wagoner, *ApJ* **278**, 345 (1984).
- [23] B. P. Abbott, R. Abbott, R. Adhikari, P. Ajith, B. Allen, G. Allen, R. S. Amin, S. B. Anderson, W. G. Anderson, M. A. Arain, and et al., *Reports on Progress in Physics* **72**, 076901 (2009), arXiv:0711.3041 [gr-qc].
- [24] The LIGO Scientific Collaboration and The Virgo Collaboration, *ArXiv e-prints* (2012), arXiv:1203.2674 [gr-qc].
- [25] B. P. Abbott, R. Abbott, T. D. Abbott, M. R. Abernathy, F. Acernese, K. Ackley, C. Adams, T. Adams, P. Addesso, R. X. Adhikari, and et al., *Physical Review Letters* **116**, 131103 (2016), arXiv:1602.03838 [gr-qc].
- [26] B. P. Abbott, R. Abbott, T. D. Abbott, M. R. Abernathy, F. Acernese, K. Ackley, C. Adams, T. Adams, P. Addesso, R. X. Adhikari, and et al., *Physical Review Letters* **116**, 061102 (2016), arXiv:1602.03837 [gr-qc].
- [27] B. P. Abbott, R. Abbott, T. D. Abbott, M. R. Abernathy, F. Acernese, K. Ackley, C. Adams, T. Adams, P. Addesso, R. X. Adhikari, and et al., *Physical Review Letters* **116**, 241103 (2016), arXiv:1606.04855 [gr-qc].
- [28] The LIGO Scientific Collaboration, the Virgo Collaboration, B. P. Abbott, R. Abbott, T. D. Abbott, S. Abraham, F. Acernese, K. Ackley, C. Adams, R. X. Adhikari, and et al., *arXiv e-prints* (2018), arXiv:1811.12907 [astro-ph.HE].
- [29] B. P. Abbott, R. Abbott, T. D. Abbott, F. Acernese, K. Ackley, C. Adams, T. Adams, P. Addesso, R. X. Adhikari, V. B. Adya, and et al., *Physical Review Letters* **119**, 161101 (2017), arXiv:1710.05832 [gr-qc].
- [30] P. Jaranowski, A. Królak, and B. F. Schutz, *Physical Review D* **58**, 063001 (1998).
- [31] B. Abbott, R. Abbott, R. Adhikari, J. Agresti, P. Ajith, B. Allen, R. Amin, S. B. Anderson, W. G. Anderson, M. Arain, and et al., *Phys. Rev. D* **76**, 082001 (2007), gr-qc/0605028.
- [32] J. Aasi, B. P. Abbott, R. Abbott, T. Abbott, M. R. Abernathy, F. Acernese, K. Ackley, C. Adams, T. Adams, P. Addesso, and et al., *Phys. Rev. D* **91**, 062008 (2015), arXiv:1412.0605 [gr-qc].
- [33] E. Goetz and K. Riles, *Classical and Quantum Gravity* **28**, 215006 (2011), arXiv:1103.1301 [gr-qc].
- [34] J. Aasi, B. P. Abbott, R. Abbott, T. Abbott, M. R. Abernathy, T. Accadia, F. Acernese, K. Ackley, C. Adams, T. Adams, and et al., *Phys. Rev. D* **90**, 062010 (2014), arXiv:1405.7904 [gr-qc].
- [35] G. D. Meadors, E. Goetz, and K. Riles, *Classical and Quantum Gravity* **33**, 105017 (2016), arXiv:1512.02105 [gr-qc].
- [36] S. W. Ballmer, *Classical and Quantum Gravity* **23**, S179 (2006).
- [37] B. Abbott, R. Abbott, R. Adhikari, J. Agresti, P. Ajith, B. Allen, R. Amin, S. B. Anderson, W. G. Anderson, M. Arain, and et al., *Phys. Rev. D* **76**, 082003 (2007), astro-ph/0703234.
- [38] J. Abadie, B. P. Abbott, R. Abbott, M. Abernathy, T. Accadia, F. Acernese, C. Adams, R. Adhikari, P. Ajith, B. Allen, G. S. Allen, E. Amador Ceron, R. S. Amin, S. B. Anderson, W. G. Anderson, F. Antonucci, and et al. (LIGO Scientific Collaboration and Virgo Collaboration), *Phys. Rev. Lett.* **107**, 271102 (2011).
- [39] B. P. Abbott, R. Abbott, T. D. Abbott, M. R. Abernathy, F. Acernese, K. Ackley, C. Adams, T. Adams, P. Addesso, R. X. Adhikari, and et al., *Physical Review Letters* **118**, 121102 (2017), arXiv:1612.02030 [gr-qc].
- [40] B. P. Abbott, R. Abbott, T. D. Abbott, F. Acernese, K. Ackley, C. Adams, T. Adams, P. Addesso, R. X. Adhikari, V. B. Adya, and et al., *Phys. Rev. D* **95**, 122003 (2017), arXiv:1704.03719 [gr-qc].
- [41] J. T. Whelan, S. Sundaresan, Y. Zhang, and P. Peiris, *Phys. Rev. D* **91**, 102005 (2015), arXiv:1504.05890 [gr-qc].
- [42] S. Dhurandhar, B. Krishnan, H. Mukhopadhyay, and J. T. Whelan, *Phys. Rev. D* **77**, 082001 (2008), arXiv:0712.1578 [gr-qc].
- [43] B. P. Abbott, R. Abbott, T. D. Abbott, F. Acernese, K. Ackley, C. Adams, T. Adams, P. Addesso, R. X. Adhikari, V. B. Adya, and et al., *ApJ* **847**, 47 (2017), arXiv:1706.03119 [astro-ph.HE].
- [44] M. deKool and U. Anzer, *Monthly Notices of the Royal Astronomical Society (ISSN 0035-8711)* **262**, 726 (1993).
- [45] A. Baykal and H. Oegelman, *Astronomy and Astrophysics (ISSN 0004-6361)* **267**, 119 (1993).
- [46] L. Bildsten, D. Chakrabarty, J. Chiu, M. H. Finger, D. T. Koh, R. W. Nelson, T. A. Prince, B. C. Rubin, D. M. Scott, M. Stollberg, B. A. Vaughan, C. A. Wilson, and R. B. Wilson, *The Astrophysical Journal Supplement Series* **113**, 367 (1997).
- [47] A. L. Watts, B. Krishnan, L. Bildsten, and B. F. Schutz, *MNRAS* **389**, 839 (2008), arXiv:0803.4097.
- [48] A. Mukherjee, C. Messenger, and K. Riles, *Phys. Rev. D* **97**, 043016 (2018), arXiv:1710.06185 [gr-qc].
- [49] P. Leaci and R. Prix, *Phys. Rev. D* **91**, 102003 (2015), arXiv:1502.00914 [gr-qc].
- [50] S. Suvorova, L. Sun, A. Melatos, W. Moran, and R. J. Evans, *Phys. Rev. D* **93**, 123009 (2016), arXiv:1606.02412 [astro-ph.IM].
- [51] S. Suvorova, P. Clearwater, A. Melatos, L. Sun, W. Moran, and R. J. Evans, *Phys. Rev. D* **96**, 102006 (2017), arXiv:1710.07092 [astro-ph.IM].
- [52] C. Messenger, *LIGO Report T1000195* (August 2011).
- [53] G. D. Meadors, E. Goetz, K. Riles, T. Creighton, and F. Robinet, *Phys. Rev. D* **95**, 042005 (2017), arXiv:1610.09391 [gr-qc].
- [54] A. Viterbi, *IEEE Transactions on Information Theory* **13**, 260 (1967).
- [55] R. Prix and B. Krishnan, *Classical and Quantum Gravity* **26**, 204013 (2009), arXiv:0907.2569 [gr-qc].
- [56] L. Sammut, C. Messenger, A. Melatos, and B. J. Owen, *Phys. Rev. D* **89**, 043001 (2014), arXiv:1311.1379 [gr-qc].
- [57] J. Aasi, B. P. Abbott, R. Abbott, T. Abbott, M. R. Abernathy, F. Acernese, K. Ackley, C. Adams, T. Adams, P. Addesso, and et al., *Phys. Rev. D* **91**, 062008 (2015), arXiv:1412.0605 [gr-qc].
- [58] L. Wang, D. Steeghs, D. K. Galloway, T. Marsh, and J. Casares, *MNRAS* **478**, 5174 (2018), arXiv:1806.01418 [astro-ph.HE].
- [59] D. Steeghs and J. Casares, *ApJ* **568**, 273 (2002), astro-ph/0107343.
- [60] C. Messenger, H. J. Bulten, S. G. Crowder, V. Dergachev, D. K. Galloway, E. Goetz, R. J. G. Jonker, P. D. Lasky, G. D. Meadors, A. Melatos, S. Premachandra, K. Riles, L. Sammut, E. H. Thrane, J. T. Whelan, and Y. Zhang, *Phys. Rev. D* **92**, 023006 (2015), arXiv:1504.05889 [gr-qc].

- [61] C. F. Bradshaw, E. B. Fomalont, and B. J. Geldzahler, *ApJ* **512**, L121 (1999).
- [62] E. B. Fomalont, B. J. Geldzahler, and C. F. Bradshaw, *ApJ* **558**, 283 (2001), astro-ph/0104372.
- [63] R. Prix, LIGO Report T0900149 (June 2011).
- [64] LIGO Scientific Collaboration, “LIGO Algorithm Library - LALSuite,” free software (GPL) (2018).
- [65] K. Wette, *Phys. Rev. D* **85**, 042003 (2012).
- [66] B. Abbott, R. Abbott, R. Adhikari, J. Agresti, P. Ajith, B. Allen, R. Amin, S. B. Anderson, W. G. Anderson, M. Arain, and et al., *Phys. Rev. D* **76**, 082001 (2007), gr-qc/0605028.
- [67] P. B. Covas, A. Effler, E. Goetz, P. M. Meyers, A. Neunzert, M. Oliver, B. L. Pearlstone, V. J. Roma, R. M. S. Schofield, and V. B. Adya, *Phys. Rev. D* **97**, 082002 (2018), arXiv:1801.07204 [astro-ph.IM].
- [68] B. P. Abbott, R. Abbott, T. D. Abbott, M. R. Abernathy, F. Acernese, K. Ackley, C. Adams, T. Adams, P. Addesso, R. X. Adhikari, and et al., *Physical Review Letters* **118**, 121101 (2017), arXiv:1612.02029 [gr-qc].
- [69] H. Ritter and U. Kolb, *A&A* **404**, 301 (2003), astro-ph/0301444.
- [70] L. Sammut, *Gravitational waves from low-mass X-ray binaries: a search for Scorpus X-1*, Ph.D. thesis, The University of Melbourne (2015).
- [71] A. Patruno and A. L. Watts, *ArXiv e-prints* (2012), arXiv:1206.2727 [astro-ph.HE].